Strengthening of In-Plane and Out-of-Plane Capacity of Thin Clay Masonry Infills Using Textile- and Fiber-Reinforced Mortar

Massimiliano Minotto, S.M.ASCE[1]; Nicolò Verlato, Ph.D.[2]; Marco Donà, Ph.D., M.ASCE[3]; and Francesca da Porto, Ph.D.[4]

Abstract: This paper presents an overview of the experimental results obtained by combined in-plane/out-of-plane (IP/OOP) tests carried out on reinforced concrete (RC) frames infilled with thin clay masonry walls. After preliminary characterization tests on building materials, combined IP/OOP tests on eight full-scale, one-bay, one-story infilled RC frames were carried out. Three external strengthening solutions were investigated considering three types of lime-based plasters, reinforced by means of dispersed fibers and/or bidirectional basalt meshes, applied on both sides of each wall. The experimental results of the tested frames are presented, discussed, and compared to evaluate the performance and the effectiveness of each strengthening solution. **DOI: 10.1061/(ASCE)CC.1943-5614.0001067**. *© 2020 American Society of Civil Engineers*.

Author keywords: Clay masonry infills; Textile-reinforced mortars (TRM); Fiber-reinforced mortars (FRM); Experimental tests; Combined in-plane/out-of-plane behavior; Infilled RC frames.

Introduction

The construction of reinforced concrete (RC) frames with thin clay masonry infill walls represents a widespread building practice in many European countries and worldwide (INSYSME 2014). These types of infill walls, also used as internal partition walls and classified as nonstructural elements, are often neglected in the current design procedures. During earthquakes, the seismic action affects these nonstructural walls, causing relevant economic losses (Chiozzi and Miranda 2017; De Martino et al. 2017; Di Ludovico et al. 2017a, b) and loss of building functionality (Dolce and Goretti 2015) in medium to severe earthquakes. Among the most relevant seismic events, it is possible to mention Loma Prieta (1989) and Northridge (1994) in California where extensive damage to nonstructural elements, in buildings with slight structural damage, accounted for a total amount of about $30 million (Vicente et al. 2010).

The out-of-plane (OOP) load can induce partial or total collapse of the infill walls, which may occur also for low seismic intensities. The brittle behavior of clay masonry infill walls leads to an uncontrolled collapse that may occur without any warning, representing a serious hazard for human lives. Furthermore, the in-plane (IP) damage of the infill, induced by the RC frame deformation, yields to a reduction of the OOP strength, thus increasing the probability of infill out-of-plane ejection (Donà et al. 2017, 2019). As a consequence, the seismic vulnerability of infill walls increases considering their combined IP/OOP response. The damage observed after recent seismic events is a demonstration of this problem, e.g., L'Aquila 2009, Italy (Bazzurro et al. 2009; Ricci et al. 2011; Braga et al. 2011); Lorca 2011, Spain (Hermanns et al. 2014; De Luca et al. 2014); Simav 2011, Turkey (Doğangün et al. 2013); Emilia 2012, Italy (Penna et al. 2014; Verderame et al. 2014); Kefalonia 2014, Greece (Manos et al. 2015); and Central Italy 2016 (Masi et al. 2017, 2019; Fragomeli et al. 2017; De Risi et al. 2018).

From the second-half of the 20th century, several experimental campaigns (among the others, Thomas 1952; Polyakov 1960; Holmes 1961; Stafford-Smith 1962; Mainstone and Weeks 1970; Mainstone 1971; Fiorato et al. 1970; Zarnic and Tomazevic 1988; Mehrabi et al. 1994, 1996; Crisafulli 1997; Anil and Altin 2007; Blackard et al. 2009; Kakaletsis et al. 2011; Bergami and Nuti 2015; Gazic and Sigmund 2016) focused on the IP behavior of infill walls, investigating the formation of the strut mechanism, the infill–frame (IF) interaction, and the IF overall response.

Few experimental studies focused on the OOP response of unreinforced infill walls (Drysdale and Essawy 1988; Dawe and Seah 1989; Dafnis et al. 2002; Tu et al. 2010), whereas a consistent number of works developed and experimentally investigated various strengthening solutions to improve the OOP performance of masonry infill walls, to avoid brittle collapse. Tumialan et al. (2003), Saatcioglu et al. (2005), El-Dakhakhni et al. (2006), Kalali (2012) and Lunn and Rizkalla (2011) introduced the application of fiber-reinforced polymer (FRP) sheets eternally bonded with organic matrixes (or epoxy resins). The reduced thickness, high stiffness, and relative ease of application give to FRP a huge range of application; nevertheless, to improve the physical and mechanical compatibility with masonry, further retrofitting techniques, based on textile-reinforced mortar (TRM), were developed.

The most common reinforcing textiles are bidirectional composite meshes made of steel or natural/mineral fibers (e.g., flax, hemp,

[1]Ph.D. Student, Dept. of Civil, Architectural and Environmental Engineering, Univ. of Padova, Via Marzolo 9, 35131 Padova, Italy. Email: massimiliano.minotto@dicea.unipd.it

[2]Research Fellow, Dept. of Civil, Architectural and Environmental Engineering, Univ. of Padova, Via Marzolo 9, 35131 Padova, Italy. Email: nicolo.verlato@dicea.unipd.it

[3]Post-Doc, Earthquake Engineering Research & Test Center, Guangzhou Univ., Guang Yuan Zhong Rd. 248, 510405 Guangzhou, China (corresponding author). Email: marcko.d@gmail.com

[4]Full Professor, Dept. of Geosciences, Univ. of Padova, Via Gradenigo 6, 35131 Padova, Italy. Email: francesca.daporto@unipd.it

Note. This manuscript was submitted on December 24, 2019; approved on May 27, 2020; published online on August 18, 2020. Discussion period open until January 18, 2021; separate discussions must be submitted for individual papers. This paper is part of the ***Journal of Composites for Construction***, © ASCE, ISSN 1090-0268.

basalt), carbon, glass, and polyester, applied with inorganic matrixes directly on the masonry surface. The effectiveness of TRMs applied on non-load-bearing masonry infill walls has been experimentally confirmed by Papanicolaou et al. (2007), Kakaletsis et al. (2011), Vasconcelos et al. (2012), Martins et al. (2015), Koutas and Bournas (2019), and De Risi et al. (2019). An extended experimental campaign was carried out by Valluzzi et al. (2014) to compare the FRP and TRM strengthening solutions and evaluate their effectiveness.

Only a relatively recent series of studies evaluated the interaction of the out-of-plane behavior of masonry infill walls with the concurring effects of in-plane damage. In particular, the earlier works of Angel et al. (1994), Flanagan and Bennett (1999), Calvi and Bolognini (2001), and Furtado et al. (2016) were the first to deal with this issue. They demonstrated how the OOP capacity degrades as the IP displacement demand increases, and in some cases, they also tested some reinforcement/strengthening techniques, such as horizontal joint reinforcement or external application of ferrocement jacketing.

More recently, also Ricci et al. (2018) dealt with the combined IP/OOP behavior of weak clay infill walls, studying the response of original infill walls in unreinforced conditions. Some other works concentrated on the use of horizontal joint reinforcement or ferrocement or other steel devices (Pereira et al. 2011; Silva et al. 2016), whereas others also tested strengthened solutions based on the external application of fiber-reinforced or textile-reinforced mortars (da Porto et al. 2015; Ismail et al. 2018; Sagar et al. 2019).

Lastly, a more recent series of works studied the combined IP/OOP behavior of more robust, eventually internally reinforced with steel bars, clay masonry infill walls (da Porto et al. 2013; Vintzileou et al. 2016; Palieraki et al. 2018), and a consistent number of works has focused on the development of innovative solutions to increase the infill wall ductility and/or decrease the infill wall/RC frame interaction (Mohammadi and Akrami 2010; Mohammadi et al. 2011; Baio Dias et al. 2014; Preti et al. 2015; da Porto et al. 2016; Verlato et al. 2016; Morandi et al. 2018; Marinković and Butenweg 2019).

These researches concerned different types of masonry infill walls to be used for new constructions. In this context, the EN 1998-1 (CEN 2004) simplistically suggests to pay particular attention to infill walls characterized by a slenderness ratio greater than 15, and to adopt measures to improve both IP and OOP behavior of the infill walls, such as light wire meshes on one face of the wall, wall ties fixed to the columns, and concrete post and belts. The use of light plaster meshes on two faces of the infill walls, interconnected through the masonry thickness and to the frame elements, or the use of bed-joint reinforcement, is also suggested by the more recent Italian Standard (Circ. 2019 no. 7, MIT 2019), as a defensive measure against OOP collapse. However, recent earthquakes demonstrated the ineffectiveness of some of these measures (e.g., the concrete post and belts, Vintzileou and Palieraki 2007), and in some other cases, these measures can be hardly applied for improving existing masonry infill walls. In addition, both codes do not explicitly refer to the problems of IP/OOP interaction.

Therefore, this research work focuses on the experimental characterization of three FRM/TRM strengthening solutions, designed for strengthening thin masonry infill walls in existing buildings. The reinforcement was externally applied on both sides of the masonry panel. The experimental campaign consisted of tests for characterizing the building materials and combined IP/OOP tests on real-scale specimens with strengthened infill walls. Eight full-scale, one-bay, one-story infilled RC frames were tested by means of quasi-static cyclic procedures to evaluate the damage progression due to IP cyclic displacements and the effect on the OOP response. The three solutions are compared in terms of envelope curves of the hysteresis loops, IP damage distribution, OOP force–displacement curves and, finally, in terms of OOP strength reduction along with the increase of IP interstory drift. Lastly, a discussion on possible design formulations for this type of strengthening solutions is given.

Description of the Strengthened Specimens

The seismic performance of three FRM/TRM strengthening solutions were experimentally investigated through combined IP/OOP tests carried out at the Laboratory of the University of Padova. The specimens were full-scale RC frame (one-bay and one-story) fully infilled with masonry panels. Each infill wall was made of clay bricks with horizontal holes (60% holes percentage) and dimensions of $250 \times 120 \times 250$ mm^3 (length × width × height). According to EN 1996-1-1 (CEN 2005), clay units were of Group 4. The mechanical properties of the blocks were stated by the manufacturer according to EN 771-1 (CEN 2015); the average compressive strengths, parallel and orthogonal to the holes, were equal to 8.0 and 2.0 N/mm^2, respectively. The masonry walls were built with both horizontal (12 mm thick) and vertical (8.8 mm thick) joints, fully filled with mortar of declared class M5 (EN 998-2, CEN 2016b). Each infill wall had a thickness of 150 mm considering that it was rendered on both façades with a 15 mm thick plaster layer. A total number of eight specimens, strengthened with three reinforcing solutions identified as *F*, *FB*, and *RBB*, were experimentally investigated. Fig. 1 shows the details of each strengthening solution, and Fig. 2 shows some details of the construction phases.

- *Strengthening type F (fiber plaster)*: characterized by a 15 mm layer of FRP containing alkali-resistant (AR) and corrosion-resistant glass fibers with a high content (above 16%) of zirconium oxide. The plaster is of class CS III (EN 998-1, CEN 2016a), with a characteristic compressive strength at 28 days of 5.0 MPa, made of natural hydraulic lime (NHL 3.5) with a quite fine grading (0÷1.8 mm). The plaster was applied directly on the raw masonry surface, without any reinforcing textile mesh.
- *Strengthening type FB (fiber plaster and basalt mesh)*: characterized by the same type of plaster used for strengthening type *F*. The only difference is that a balanced biaxial mesh, made of alkali-resistant basalt fibers, was embedded into the two external plaster layers, each 15 mm thick. The basalt net, produced with square mesh size 22×22 mm^2, is characterized by an equivalent thickness of 0.023 mm, a characteristic tensile strength greater than 1,600 MPa, a Young's modulus of 56,000 MPa, a minimum value of ultimate strain of 2.5%, and a weight of 0.12 kg/m^2; the failure load is therefore greater than 30 kN/m (information certified by the manufacturer). Like the previous strengthening type *F*, the plaster was applied on the raw masonry surface.
- *Strengthening type RBB (render, basalt mesh, and helicoidal bars)*: composed of a first plaster layer (shortly named *R*) of class CS II and thickness 10 mm, with quite fine grading (0÷1.4 mm) and made of pure NHL 3.5, directly applied on the raw masonry surface to simulate the presence of a preexisting, low-quality plaster. Subsequently, a second plaster layer of class CS IV and thickness 5 mm was applied on the first one with interposition of the previously mentioned balanced biaxial basalt fiber mesh. The second plaster type is a smoothing–levelling plaster type NHL 3.5 with the same grading of the initial one. In addition, the strengthening was fixed to the RC frame top beam by means of 8 Ø8 mm helicoidal stainless steel ties, which are made of steel type AISI316 and have a characteristic tensile failure load greater than 12.7 kN.

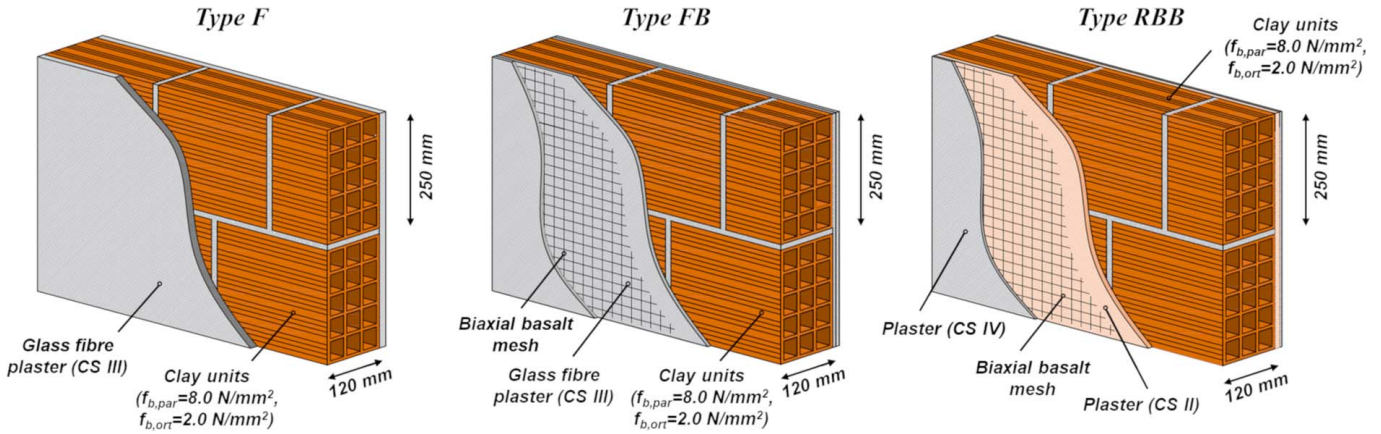

Fig. 1. Strengthening solutions (*F*, *FB*, *RBB*).

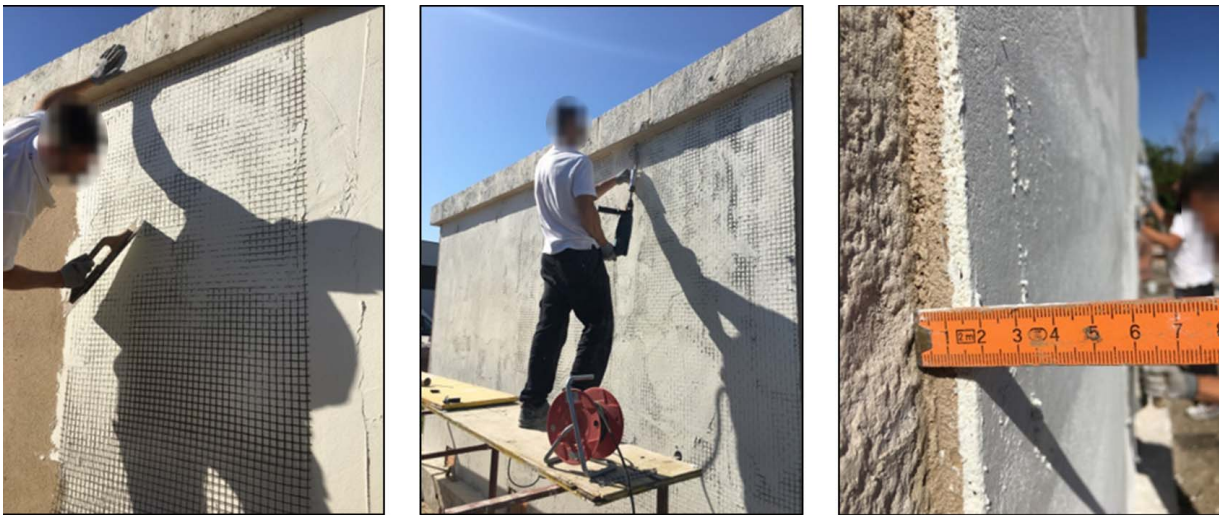

Fig. 2. Application of *RBB*. (Images by Nicolò Verlato.)

The basalt mesh (used in the *FB* and *RBB* solutions) is supplied in 1 m-wide rolls; it was embedded into the plaster layer with a vertical strip arrangement and an overlap width of 20 cm, without adopting any anchoring device to the RC frame besides the helicoidal bars in the *RBB* solution. These helicoidal bars were dry installed, with an inclination of 45° and a penetration depth in the beam of about 5 cm. After inserting the bars into the beam, they are bent to be embedded into the second plaster layer. Compared with the use of traditional bars, helicoidal bars are more convenient, as they do not have to be grouted.

These bars act only as further restraints, avoiding the rigid rotation of the infill panel and thus allowing a better activation of the resistant OOP mechanism (vertical arching and/or vertical bending). These bars were used in the *RBB* reinforcement only, which being applied on an existing (poor) plaster layer, is the one that needs the greater aid to improve the OOP capacity of the masonry panel, as well as to reduce its IP damage. In the other solutions (*F* and *FB*), which were applied on the masonry and column surface directly, it was decided to rely on the new plaster adherence only. In this case, the main aim was to check whether the reduced time- and cost-consuming strengthening solutions *F* and *FB* could still increase the OOP capacity of the infill walls, although not significantly improving the fragile OOP collapse mode.

Table 1 summarizes the specimens and the type of test that was carried out. For each type of strengthening solution, one specimen was directly (without previous in-plane damage) tested out-of-plane, by monotonic loading on eight points. Other three specimens were in-plane tested imposing incremental cyclic displacements at the frame top beam, until 1.2% drift, and only after this IP damaging, they were tested out-of-plane until collapse. The same test procedure was applied, only for strengthening type *FB* and *RBB*, also on specimens tested until 0.5% drift.

The name of the specimens in Table 1 is given by the type of strengthening solution (*F*, *FB*, and *RBB*) and by the maximum in-plane drift θ_{max} to which the sample was cyclically tested before the out-of-plane monotonic test.

Material Characterization

Flexural and compression tests on plaster specimens and on masonry assemblages were performed to characterize the mechanical properties of the masonry substrate and of the strengthening materials. Other common tests, such as compression tests on clay units, were not carried out, as the same units had already been tested during a previous experimental campaign (Valluzzi et al. 2014).

Table 1. Experimental specimens

Specimen	Preexisting plaster	Strengthening	Test type
F.00	—	Fiber plaster of class CS III	OOP
F.12			IP ($\theta_{max} = 1.2\%$) + OOP
FB.00	—	Fiber plaster of class CS III + basalt fiber mesh	OOP
FB.05			IP ($\theta_{max} = 0.5\%$) + OOP
FB.12			IP ($\theta_{max} = 1.2\%$) + OOP
RBB.00	Class CS II	Class CS IV + basalt fiber mesh + helicoidal stainless steel ties	OOP
RBB.05			IP ($\theta_{max} = 0.5\%$) + OOP
RBB.12			IP ($\theta_{max} = 1.2\%$) + OOP

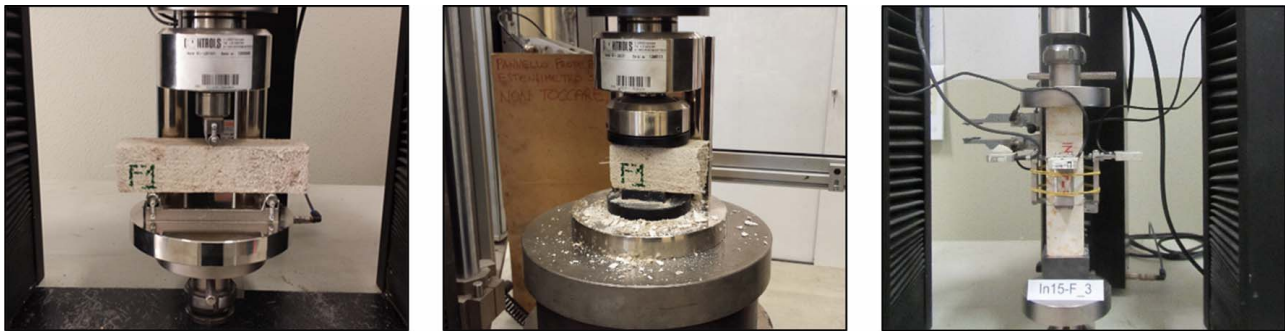

(a) (b) (c)

Fig. 3. (a) Flexural; (b) compressive; and (c) elastic modulus characterization tests on plaster specimens.

The preparation of the samples and the test procedures were in accordance to specific standard requirements.

Tests on Plasters

Plaster specimens were sampled during the construction of both the masonry assemblages to be tested in compression and the infill walls for the combined IP/OOP tests and were tested after 28 days curing, according to EN 1015-1 (CEN 1998a) and EN 13412 (CEN 2006b). With reference to the strengthening solutions described before, six specimens for each mortar type M (CS IV), F (CS III), and R (CS II) were tested. According to EN 1015-11/A1 (CEN 2006a), specimens of dimensions $160 \times 40 \times 40$ mm^3 were monotonically loaded with a uniform rate of 50 N/s to evaluate the flexural strength [Fig. 3(a)]. After the failure of the sample, the two portions were kept for the determination of the compressive strength [Fig. 3(b)] using the same testing machine of the previous flexural tests and applying a constant loading rate of 200 or 400 N/s until failure. No specific standards are available to conduct tests for the determination of the mortars Young's modulus; thus, the standard for hardened concrete EN 12390-13 (CEN 2013) was considered. Elastic modulus tests were carried out on one of the three prismatic specimens of each mortar sample only, measuring on each face of the specimen the vertical strains during several loading cycles [Fig. 3(c)]. Table 2 lists the average values of flexural strength, cubic compressive strength, and elastic modulus of the tested plaster.

Tests on Masonry Assemblages

To characterize the basic mechanical properties of the masonry constituting the infill wall systems analyzed in this work, 12 masonry specimens with a shape ratio b:h = 1:1 (dimensions 775×780 mm^2, Fig. 4) were tested in compression following the standard EN 1052-1 (CEN 1998b). The load was applied orthogonally to the masonry unit holes, in displacement control, with a velocity of 1.0 mm/min. As in the case of the subsequent flexural tests, one type of specimen was built with the low-quality plaster type *R* and without any type of reinforcement, whereas the other two specimen types were made with strengthening types *RBB* and *F*.

Table 2. Mechanical properties of plasters (CoV in brackets)

Plaster type	Flexural strength [N/mm^2]	Compressive strength [N/mm^2]	Elastic modulus [kN/mm^2]
M	3.9 (23.3%)	12.8 (29.4%)	5.9 (19.7%)
F	2.6 (28.3%)	8.6 (30.4%)	7.4 (16.4%)
R	1.3 (16.1%)	3.6 (22.0%)	4.5 (10.6%)

Table 3 shows a summary of the results. As expected, the compressive strength and the elastic modulus of the specimens were not significantly affected by the quality of the plaster and the presence of the basalt mesh.

Two types of flexural tests, both having plane of failure parallel to the bed joints, were conducted. The first type of test was carried out on specimens having the low-quality plaster that simulate a preexisting material, without any reinforcement. In this case, a bending test on a mortar joint was carried out, as larger specimens could have collapsed under the effect of the dead-load only. Conversely, in the case of specimens with a strengthening system applied, an ordinary four-point bending test was carried out.

- *Mortar joint bending tests:* nine masonry assemblages with plaster type *R* (CS II) and dimensions $250 \times 515 \times 150$ mm^3 [Fig. 5(a)] were tested applying the monotonic load directly on the mortar joint. The specimens were placed on two steel supports with a diameter of 40 mm, spaced by 415 mm, and a third steel roller of the same geometry was located centrally for loading the specimen [Fig. 5(b)] under displacement control (velocity rate of 0.5 mm/min). The typical failure mode occurred along the mortar joint, as shown in Fig. 5(c). The average maximum nondimensional bending moment per meter length of specimens was 1.1 kN · mm/mm.

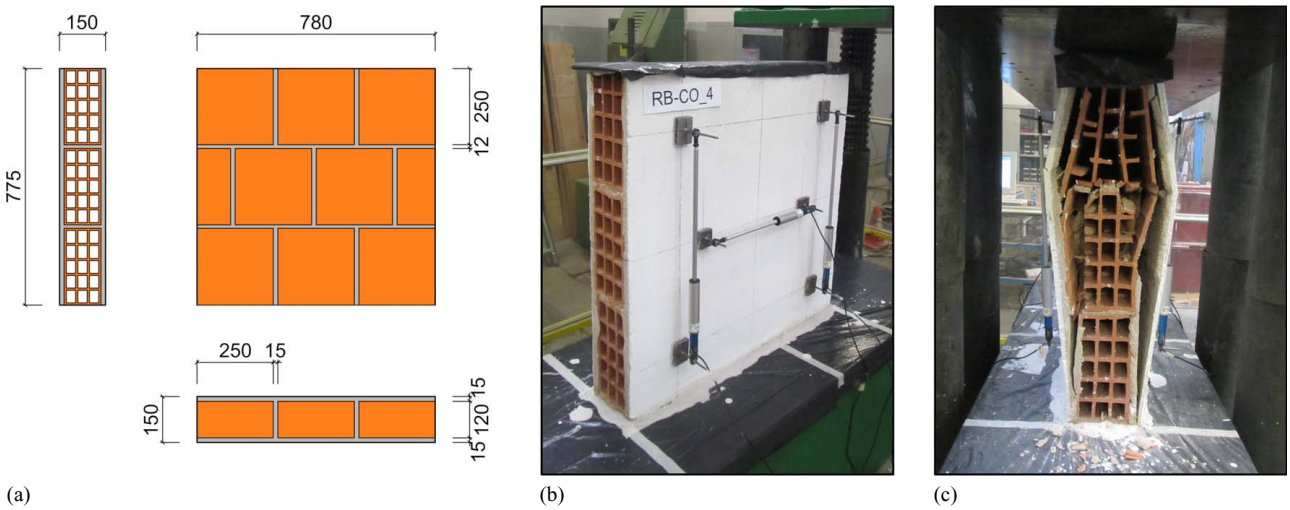

Fig. 4. Compression tests: (a) geometry with dimensions in mm; (b) test setup; and (c) failure mode.

Table 3. Compression test results (CoV in brackets)

Specimen	Max. load [kN]	Compressive strength [N/mm^2]	Elastic modulus [kN/mm^2]
R	293	2.7 (12.2%)	4,198 (12.7%)
RBB	358	2.9 (14.0%)	4,777 (22.2%)
F	325	2.8 (6.1%)	4,752 (37.5%)

Fig. 5. Flexural tests on mortar joints: (a) geometry with dimensions in mm; (b) test setup; and (c) failure mode.

- *Four-point bending tests:* four specimens of dimensions 1,300 × 390 mm^2 [Fig. 6(a)] for each type of strengthening solution (*RBB*, *FB*, *F*) were tested with plane of failure parallel to the bed joint (EN 1052-2, CEN 1999). During the application of the monotonic load, the deflection was measured by six displacement sensors [Fig. 6(b)]. Fig. 7 shows test results. In specimen type *F*, the collapse was fragile and occurred immediately after reaching peak strength. Conversely, *RBB* and *FB* showed a more controlled collapse, governed by the failure of the basalt mesh fibers along the main tensile crack [Fig. 6(c)], which developed close to one of the load application lines. The average value of the nondimensional bending moment per meter length was 2.7 kN · mm/mm in the case of specimens *F* and 3.1 kN · mm/mm in the case of *RBB* and *FB*.

Table 4 summarizes the results of the flexural tests. It is evident that the use of a low-quality plaster (*R*) and of a plaster reinforced by means of dispersed glass fibers (*F*) provides significantly different results. Indeed, despite the test results may have been partly influenced by the different test set-ups used, the obtained results reflect the difference in the basic mechanical properties of the two coating materials (see Table 2) that constitute a significant portion of the entire cross section, on both the tension and compression sides of the specimens. Conversely, once a reinforcing mesh is embedded into the plaster, the results obtained on *RBB* and *FB* are practically the same.

In-Plane/Out-of-Plane Tests Set-Up and Procedure

The combined IP-OOP tests were conducted on full-scale, one-bay, and one-story, RC frames (Fig. 8) fully infilled with the above described masonry type. The choice to adopt full-scale specimens was

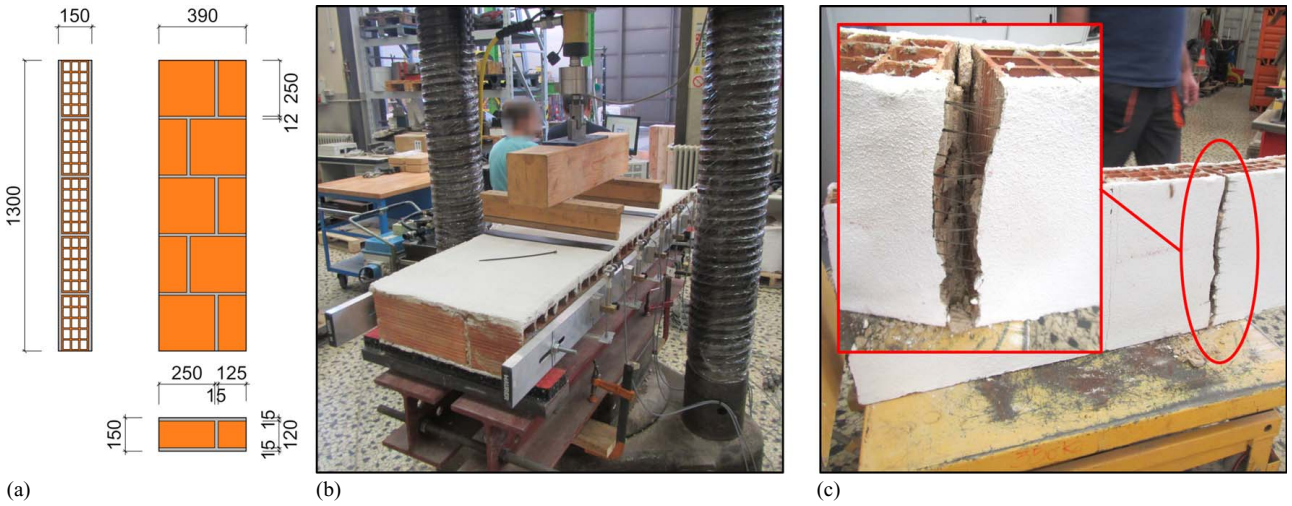

Fig. 6. Four-point bending tests: (a) geometry with dimensions in mm; (b) test setup; and (c) failure mode.

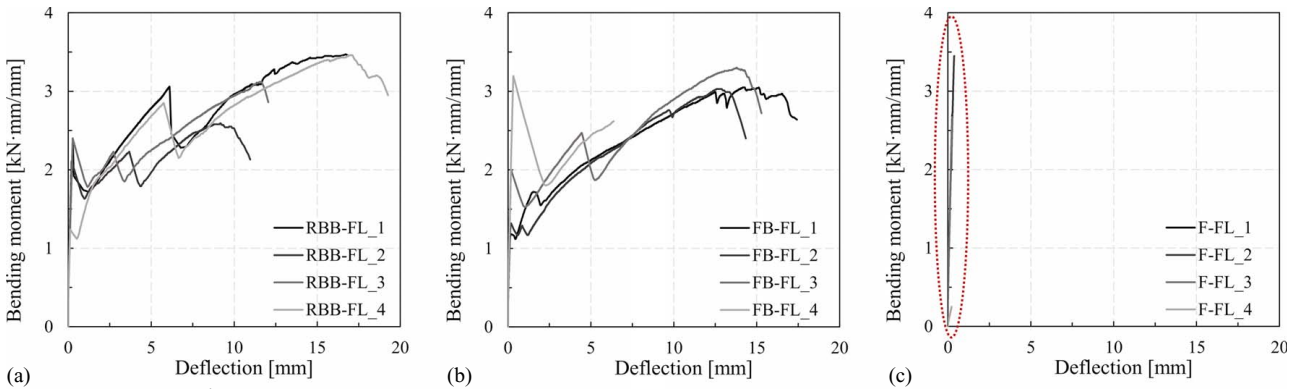

Fig. 7. Four-point bending test results: (a) *RBB*; (b) *FB*; and (c) *F* specimens.

Table 4. Flexural test results (CoV in brackets)

Specimen	Dim. less bending moment [kN]	Flexural strength [N/mm^2]
R	1.1	0.3 (30.9%)
RBB	3.1	0.9 (14.4%)
FB	3.1	0.8 (5.7%)
F	2.7	0.7 (22.0%)

made to avoid any scaling effect due to the relative stiffness ratio of the RC frame and infill wall in the scaled specimens and the real situation. The specimens were designed following the criteria described in da Porto et al. (2013), and their main characteristics are shortly reported. The infill wall dimensions were 4.15 × 2.65 mm^2 (length × height) and the RC frame was designed as part of the ground level frame of a regular three-story typical Italian residential building (class of use II) with columns spaced 4.5 m by 4.5 m and 3.0 m high storys. The frame was designed in a high ductility class (class "A" according to MIT 2008), considering a peak ground acceleration (PGA) of 0.25*g*. Concrete frame cross sections were designed to respect the hierarchy of strength.

The experimental set-up consisted of two servo-controlled hydraulic actuators placed over the beam-column nodes for applying vertical loads. The load is transferred to the columns through a self-locking device, hinged to a reaction steel beam at the top of the actuator and connected by ball-and-socket joints to the RC frame bottom beam. An axial load of 200 kN on each column was kept constant during the IP and OOP tests. One servo-controlled hydraulic actuator is placed at the height of the top beam for applying horizontal IP cyclic displacements. Lastly, the loading system for the OOP test is made of commercial steel profiles connected to another hydraulic jack. The system allows applying eight punctual forces of equal intensity at every third of the width and at each fifth of the height of the masonry infill wall.

To measure IP deformations, 11 potentiometric transducers and 1 magnetostrictive transducer were installed on the RC frame. In particular, the magnetostrictive transducer was anchored to the top beam to measure the horizontal displacements applied to the specimens and to retroactivate the horizontal actuator. In addition, to measure global OOP deflections, four potentiometric transducers and nine draw wire sensors were installed on the infill walls, and two potentiometric transducers were installed on the top beam for control purposes. Fig. 8 shows the position of the sensors for the measurement of IP/OOP deformations. Load cells were also applied on each actuator stem to measure forces and to retroactivate vertical and OOP loading actuators. Fig. 9 shows some details of the IP/OOP test set-up.

The test procedure adopted was quasi-static. For IP tests, the displacement history shown in Fig. 10(a) was applied (with a maximum stroke speed of less than 0.5 mm/s), which consists of cyclic displacements of increasing amplitude that are repeated three times for each amplitude; the target displacements were defined based on the following interstory drifts: ±0.1%; ±0.2%; ±0.3%; ±0.4%;

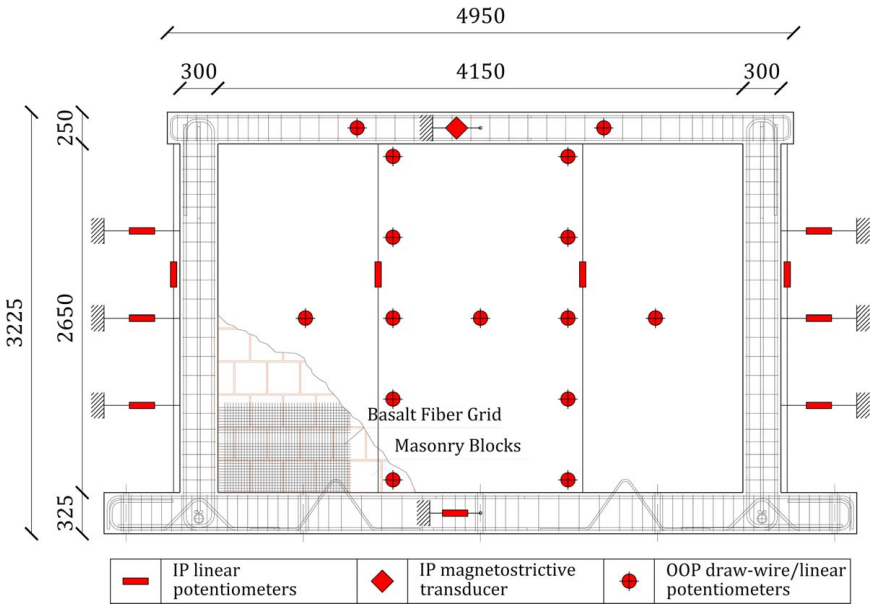

Fig. 8. RC frame geometry with dimensions in mm.

Fig. 9. Experimental setup: (a) actuators for vertical loading; (b) actuator for IP horizontal displacements; and (c) OOP thrusting system.

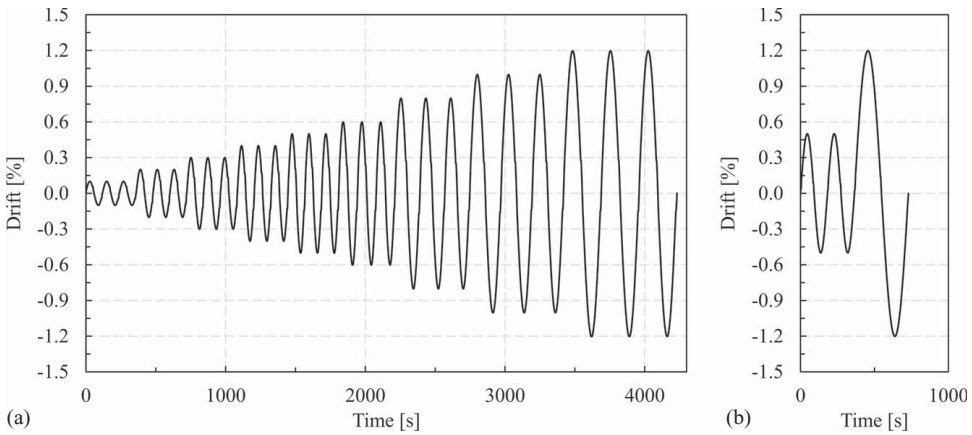

Fig. 10. IP test protocols adopted for (a) infilled frames; and (b) bare frames.

J. Compos. Constr., 2020, 24(6): 04020059

Fig. 11. Crack pattern and view of specimens at end of IP tests.

±0.5%; ±0.6%; ±0.8%; ±1.0%; ±1.2%. At the end of the IP test, the specimens were brought back to null horizontal displacement and then the OOP test was performed by applying a monotonic incremental force until the collapse of the infill. At the end of the OOP test, the infill walls were completely removed and the bare frames (BF) were tested in-plane [see Fig. 10(b)]; it was thus possible to evaluate the contribution of the RC frame to the global IP response of the infilled specimens.

Combined IP/OOP Test Results

In-Plane Tests

Fig. 11 shows the crack patterns and some detailed pictures of the observed damage at the end of the IP tests. The data acquired during the tests were used to obtain the hysteresis loops shown by Fig. 12. The hysteresis loops were not completely symmetrical due to a nonsymmetrical damage on the reverse loading cycles. However, for the strengthening type *RBB* (and *FB*), for which two specimens were tested at different maximum drift levels, it can be seen that the initial part of the two tests gives comparable results, demonstrating the reliability and repeatability of the tests.

Fig. 12 shows the force–displacement envelope curves associated with the three loading cycles. As can be seen, the execution of three loading cycles per each displacement level allows characterizing the initial response of the specimen after damage accumulation and allows checking how stable the specimen response is at each target displacement. Indeed, damage accumulation decreases rapidly as the number of cycles increases at the same drift level, becoming negligible after the third cycle. For this reason, some results (e.g., the load–drift envelope curves of the infill walls) are given on the third cycle, in order to conservatively take into account the inelastic cyclical response of a structure during an earthquake.

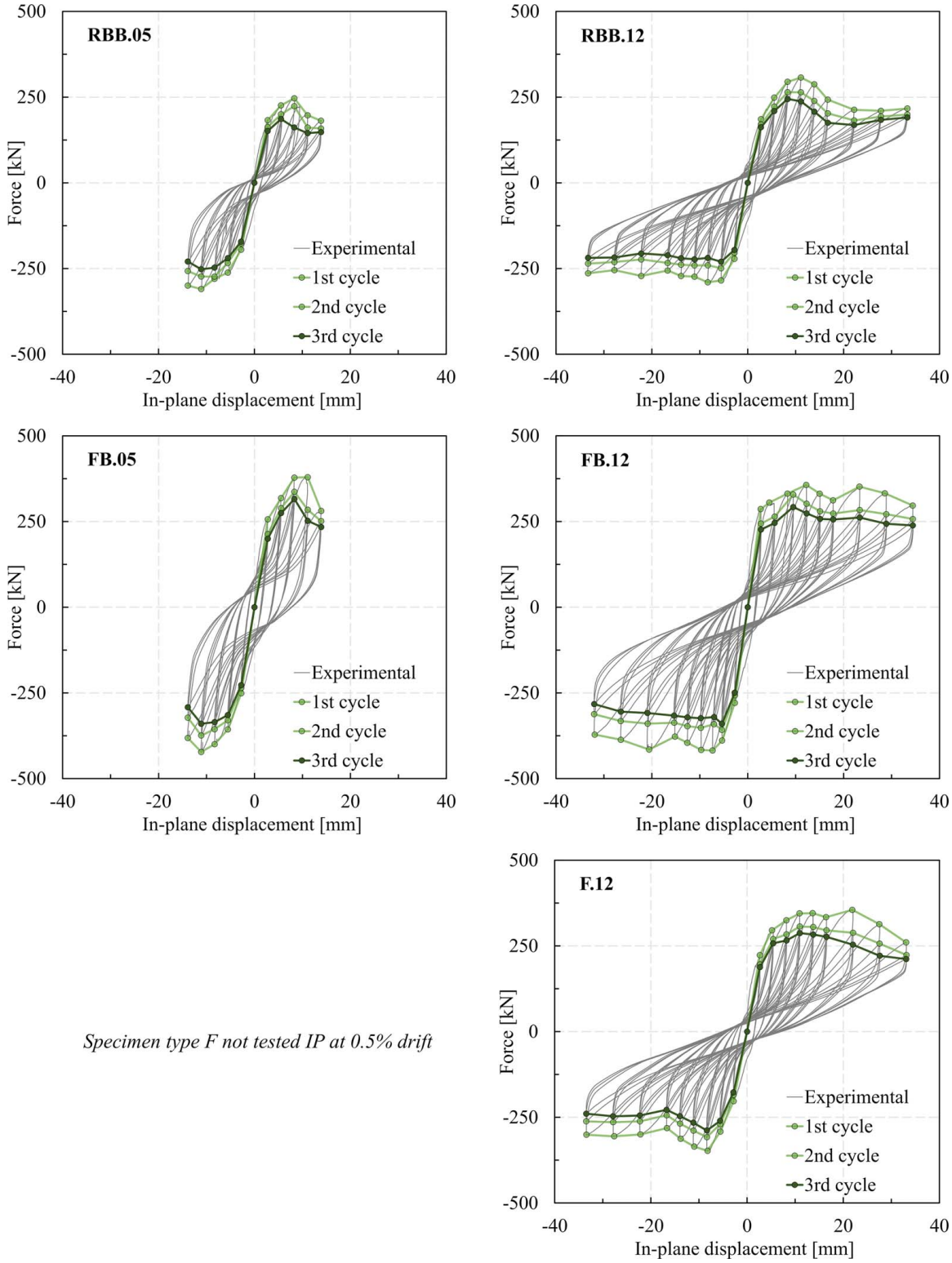

Specimen type F not tested IP at 0.5% drift

Fig. 12. Hysteresis loops and envelope curves of IP tests.

The choice of having closer target displacements in the drift range from 0% to 0.6%, where the panel undergoes the various limit states and quickly changes its stiffness, allowed to obtain accurate force–displacement curves in the most significant test phases, while maintaining reasonable testing times.

Fig. 13(a) shows the hysteresis loops and envelope curve obtained from the test of a bare frame. This test was performed after testing the associated infilled frame, and allowed to derive the IP behavior of the infill wall as the difference between the force–displacement envelope curve of the infilled frame and that of the bare frame [Fig. 13(b)]. Fig. 13 shows that the bare frame response is almost linear in the range of analyzed displacements, which means that the frame is not significantly affected by the previous test carried out on the infilled frame. This is reasonable considering that the frame was designed in high ductility class for a PGA of 0.25*g* (hence, with severe reinforcement details), and tested

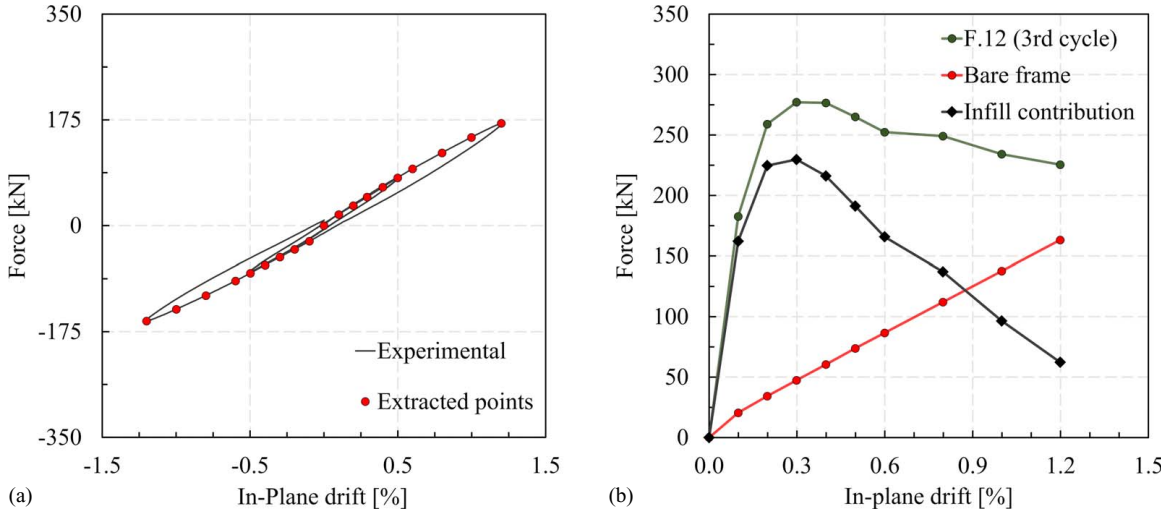

Fig. 13. (a) IP hysteresis loops of bare frame; and (b) infill wall contribution: subtraction of bare frame from infilled frame.

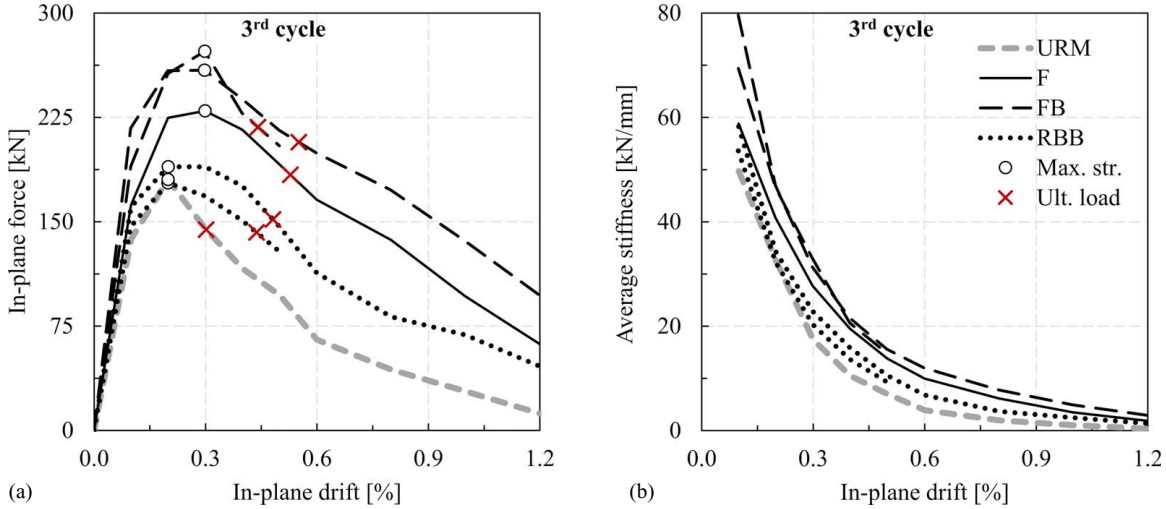

Fig. 14. IP tests (all specimens): (a) load-drift envelope curves; and (b) stiffness degradation.

up to relatively low levels of drift, at which no significant damage was visible. The obtained results can be thus considered reliable.

The IP performance of the investigated FRM/TRM solutions can therefore be compared in terms of load–drift envelope curves and stiffness degradation (Fig. 14), equivalent viscous damping ratio and energy dissipation capacity (Figs. 15 and 16), and global parameters at maximum and ultimate capacity (Table 5). Conversely, since the adopted external reinforcement systems tend to hide the internal portion of the infill walls, and thus do not allow appreciating the evolution of damage, the analysis of crack patterns was carried out at the end of the IP tests only (Fig. 11) and was not given as a function of the drift level. Further considerations and observations were then made possible by comparing all specimens with a reference unreinforced infill wall (URM), which was tested in a previous experimental campaign (da Porto et al. 2015). The URM panel was geometrically identical to this research samples and it was realized using the same type of masonry units. The external plaster layer was made of natural hydraulic lime without strengthening mesh. It was cyclically IP tested up to 1.2% drift.

Fig. 14(a) shows the force–displacement envelope curves of the infill walls, while Fig. 14(b) reports the secant stiffness degradation of the infill, due to increasing IP displacements. Figs. 15 and 16 show the comparison of the FRM/TRM solutions in terms of, respectively, equivalent viscous damping ratio (ξ) and energy dissipation capacity (E_{hyst}/E_{inp}) of the infill walls per loading cycle. The equivalent damping ratio is obtained with the simplified method proposed by Jacobsen (in 1930), i.e., as: $\xi = E_{hyst}/(4\pi E_{sto})$, where E_{hyst} = energy dissipated per-cycle and E_{sto} = elastic energy stored at the peak displacement. In particular, E_{hyst} is calculated as the sum of the products between the imposed displacement increments and the related measured loads (for the whole cycle). Instead, E_{inp} is the input energy, i.e., the total energy provided to the specimen during the test, and it is obtained with the same procedure as E_{hyst} but is limited to positive products only. Table 5 summarizes the following results: maximum IP capacity F_{max}, drift θ_{Fmax} at peak strength, infill damping ratio ξ and energy dissipation capacity E_{hyst}/E_{inp} at maximum strength, ultimate force F_{ult} evaluated as a 20% decrease of F_{max} and related drift θ_{Fult}, and the maximum stiffness K_{max}.

Observing the test results, the embedded fiber meshes seems to provide a better distribution of IP damage. Indeed, specimen *F.12*, the only one without reinforcing mesh, developed the first well-defined cracks along the infill–frame interface since 0.2% drift.

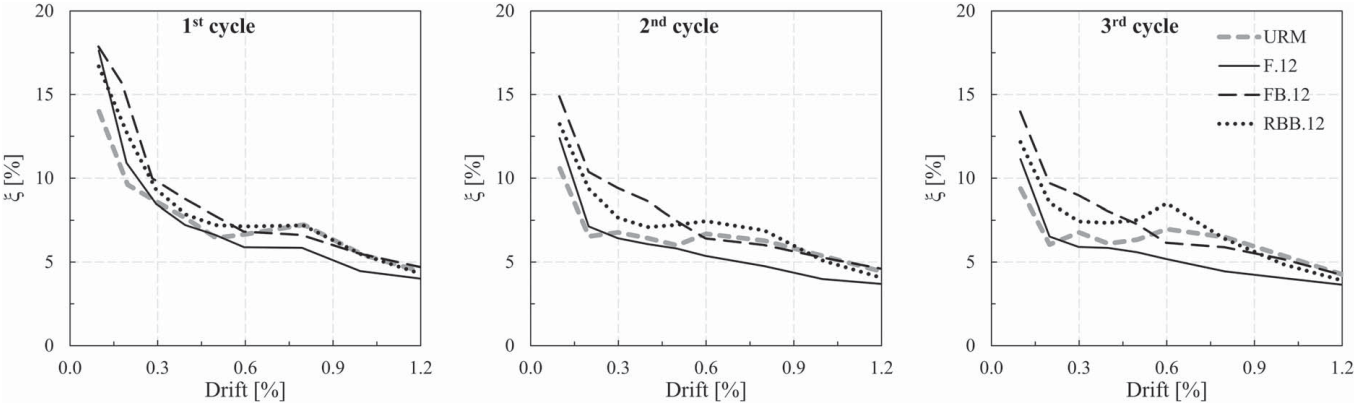

Fig. 15. IP tests (specimens $\theta = 1.2\%$): equivalent viscous damping ratio (ξ) per loading cycle.

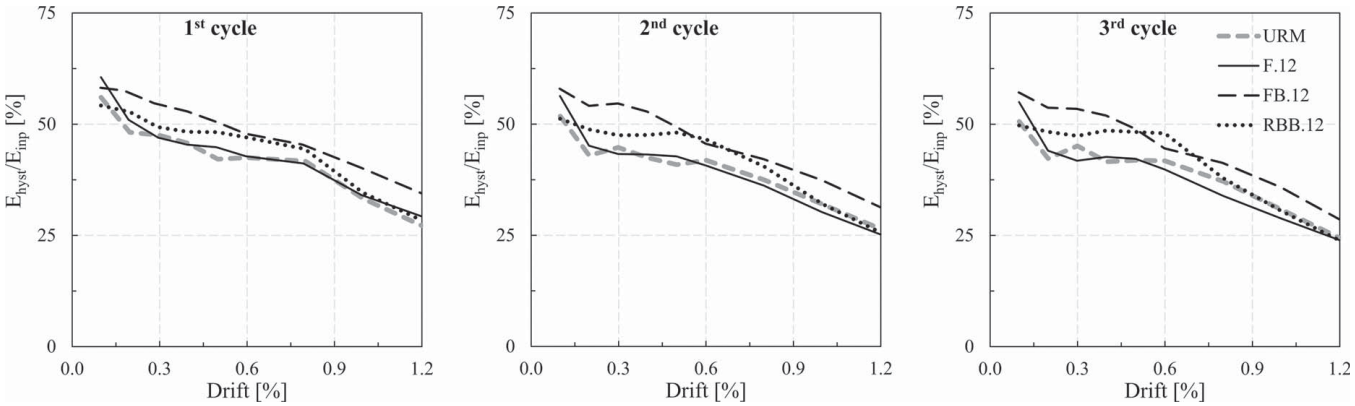

Fig. 16. IP tests (specimens $\theta = 1.2\%$): energy dissipation capacity (E_{hyst}/E_{inp}) per loading cycle.

Table 5. In-plane test results

Specimen	Maximum capacity				Ultimate capacity		K_{max} [kN/mm]	Average $\theta_{Fult}/\theta_{Fmax}$ [—]
	F_{max} [kN]	θ_{Fmax} [%]	ξ [%]	E_{hyst}/E_{inp} [%]	F_{ult} [kN]	θ_{Fult} [%]		
F.12	230	0.30	5.9	41.8	184	0.53	58.8	1.77
FB.05	273	0.30	10.6	56.0	218	0.42	69.4	1.62
FB.12	259	0.30	9.0	53.5	207	0.55	79.6	
RBB.05	178	0.20	5.7	38.5	142	0.44	53.6	2.31
RBB.12	190	0.20	8.5	48.3	152	0.48	58.3	
URM.12	181	0.20	6.0	32.7	144	0.30	49.7	1.52

Damage increased until attaining maximum drift $\theta_{Fmax} = 1.2\%$, at which widespread damage with detachment of plaster portions and crushing of masonry blocks at the infill corner was observed (see Fig. 11). The infill reached its maximum IP capacity 230 kN at 0.3% drift, and its ratio of $\theta_{Fult}/\theta_{Fmax}$ was 1.77 (Table 5). The reference unreinforced infill wall showed thin cracks and plaster detachment concentrated in the upper beam–column joint area and along the infill–frame interface up to 0.5% drift. The peak strength of 181 kN was achieved at 0.2% drift after which infill strength decreased quite sharply. At 1.2% drift, the masonry corner was disintegrated, and significative lateral portions collapsed out-of-plane (see Fig. 17). Compared with the *F.12* specimen, it had more extended damage of the wall which was not prevented by the external plaster with lower mechanical properties. In terms of IP capacity, the URM infill wall behaved similarly to the *RBB* specimens, reaching comparable peak strength at the same IP drift level (i.e., 0.2%), although the post-peak behavior of *RBB* was characterized by a more gradual strength decrease.

Indeed, in all specimens characterized by the presence of the basalt mesh (*RBB* and *FB* strengthening solutions), IP damage developed in a completely different manner. Detachment was limited to little plaster portions and the only visible cracks were at the column–infill interface. The mesh could not prevent IP damage from occurring, but it could effectively counteract masonry and plaster portions from falling off the wall (see Fig. 11).

Coupling basalt mesh with glass fiber plaster allowed reaching higher maximum strength. *FB.05* and *FB.12* reached their peak capacity of 273 and 259 kN at a drift of 0.3% and the average ratio of $\theta_{Fult}/\theta_{Fmax}$ was 1.62. As expected, the lower values of F_{max} were related to the application of the basalt mesh directly on an existing

(a) (b)

Fig. 17. Reference URM infill wall at (a) 0.3% drift; and (b) 1.2% drift.

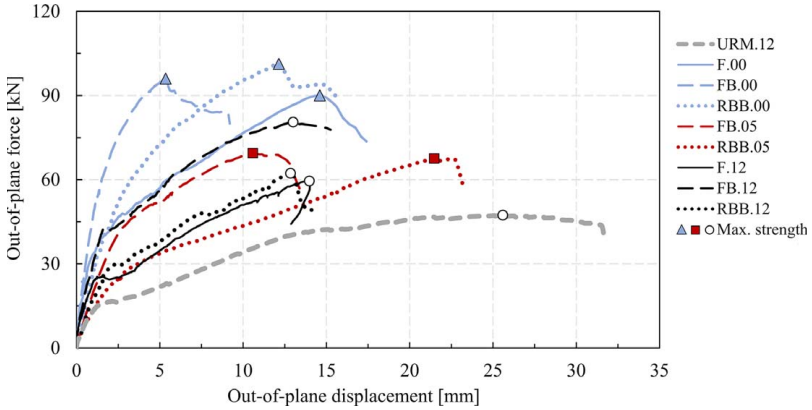

Fig. 18. OOP force-displacement curves.

plaster of lower mechanical properties. Indeed, specimens *RBB.05* and *RBB.12* reached their peak strength (178 and 190 kN respectively) at a drift value (0.2%) lower than that found for the previous solutions due to the thick low-quality plaster layer between the masonry panel and the strengthening system. For *RBB* specimens, the average ratio of $\theta_{F\text{ult}}/\theta_{F\text{max}}$ was 2.31.

The post-peak behavior is very important in evaluating the overall performance of the investigated solutions. In general, all strengthening solutions showed a better post-peak branch with respect to the URM infill wall, with higher ultimate strength (especially for *FB* and *F* solutions) and/or with a more gradual strength degradation (as shown by the average values of $\theta_{F\text{ult}}/\theta_{F\text{max}}$). In terms of stiffness degradation [Fig. 14(b)], all specimens showed similar trends and the URM infill wall, due to its significative IP damage, showed the lowest stiffness values.

Lastly, the energy dissipation capacity of the strengthening solutions with embedded mesh (*RBB* and *FB*) is greater than that of the *F* and URM cases (Figs. 15 and 16). In particular, this better performance is more evident for the loading cycles following the first and in the drift range between 0% and 0.6%, which includes the ultimate limit state of these infill walls. Considering that the *RBB* and *FB* solutions are those associated with the lowest level of observed damage (see Fig. 11), these results further confirm the overall effectiveness of these solutions. Such behavior can be explained in relation to the improved distribution of IP damage allowed by the strengthening mesh.

Out-of-Plane Tests

As previously mentioned, specimens *F.00*, *FB.00,* and *RBB.00* were tested under OOP monotonic loading without previous application of IP displacements, whereas *FB.05* and *RBB.05* were tested OOP after attaining 0.5% IP drift and *F.12*, *FB.12,* and *RBB.12* after 1.2% drift. Fig. 18 shows the force–displacement curves of the OOP tests, whereas Figs. 19–21 show the main failure modes of the eight specimens. Table 6 lists the main experimental results in terms of maximum OOP capacity F_{max}, relevant displacement $\delta_{F\text{max}}$, and observed collapse mode.

All undamaged specimens obtained similar values of maximum OOP capacity. Thanks to the combination of fiber plaster with good mechanical properties and of basalt mesh, *FB.00* had the stiffer OOP behavior, reaching its maximum capacity (96.01 kN) with an OOP deflection of 5.35 mm. *F.00* showed an initial stiffness equal to that of *FB.00* (the two specimens have the same plaster type) but, starting from 30 kN, cracking induced a significant loss of stiffness. The infill reached a capacity of 90.05 kN at 14.60 mm. Lastly, *RBB.00* showed an intermediate behavior. In this TRM solution, probably due to the low-quality plaster, it had an initial stiffness that was lower than those of *FB.00* and *F.00* but, thanks to the basalt mesh, the hardening branch developed until the peak strength of 101.31 kN, attained with an OOP deflection of 12.14 mm.

The experimental results demonstrated that IP damage is responsible for a reduction of OOP stiffness and strength. This

J. Compos. Constr., 2020, 24(6): 04020059

(a) (b) (c)

Fig. 19. OOP failure mode: (a) *F.00*; (b) *FB.00*; and (c) *RBB.00*.

(a) (b)

Fig. 20. OOP failure mode: (a) *FB.05*; and (b) *RBB.05*.

(a) (b) (c)

Fig. 21. OOP failure mode: (a) *F.12*; (b) *FB.12*; and (c) *RBB.12*.

Fig. 22. OOP failure mode of URM infill wall (da Porto et al. 2015).

Table 6. Out-of-plane test results

	Out-of-plane capacity			
Specimen	F_{max} [kN]	δ_{Fmax} [mm]	a_{eq} [g]	Failure mode
F.00	90	14.6	5.7	Material ejection
FB.00	96	5.4	6.0	Controlled
RBB.00	101	12.1	5.4	Controlled
FB.05	70	10.6	4.4	Controlled
RBB.05	68	21.5	3.6	Controlled
F.12	60	14.0	3.7	Material ejection
FB.12	81	13.0	5.1	Controlled
RBB.12	62	12.8	3.3	Controlled

means that IP damage induced lower values of maximum OOP strength with higher values of OOP deflections, as all tested specimens generally confirmed. An anomalous behavior was observed for specimen *FB.12*. Indeed, this infill wall reached an OOP capacity of 80.54 kN, which was higher than that of *FB.05* (i.e., 69.51 kN). This was caused by a more accurate construction of the infill wall, due to the fact that it was a replica of another one, that failed even before carrying out the experimental test.

Considering the observed collapse mechanisms (Figs. 19–21), the FRM solution (without the embedded basalt mesh) showed a more fragile collapse mode, characterized by the uncontrolled ejection of masonry and plaster portions [see Figs. 19(a) and 21(a)]. In addition, the URM infill wall, after being tested IP up to 1.2% drift, showed a rather fragile collapse. As shown in Fig. 22, the masonry wall subdivided into three portions separated by the diagonal cracks which had formed during the in-plane test. The effectiveness of the embedded mesh was again demonstrated by the *FB* and *RBB* TRM solutions, whose out-of-plane collapse occurred maintaining the overall integrity of the masonry panel. The reinforcing mesh is highly effective, even when it is applied directly on the existing low-quality plaster. This aspect is particularly relevant, especially in all those situations where a rapid and low impact rehabilitation intervention is required. Furthermore, the additional use of helicoidal anchorages that connect the strengthening system to the upper beam (*RBB* solution) represents a further defense against the OOP overturning of the masonry panels. It is worth noting that, despite the considerable contribution in the OOP behavior, the helicoidal bars did not significantly influence the infill IP response, both in terms of damage reduction and post-peak behavior control.

Table 6 also lists the values of OOP equivalent acceleration (a_{eq}) reached by each infill type, calculated assuming the total mass of the infill wall (variable between 1.6 and 1.9 t depending on FRM/TRM solution) as participating mass. The proposed values of a_{eq} take into account the soil amplification factor S, the position of the infill along the building height H, and the interaction between infill wall and RC frame in terms of T_a/T_1 ratio, where T_a and T_1 are the fundamental vibration period in the OOP direction of the infill and of the frame, respectively. It must be taken into account that the dynamic effects associated to the real seismic action may reduce the previous OOP strength values, obtained by means of a quasi-static test.

Influence of In-Plane Damage on Out-of-Plane Strength

Analyzing the OOP tests, the specimens tested until an IP drift level of 0.5% (*FB.05* and *RBB.05*) showed a significant OOP strength degradation (33%) compared with the specimens tested only under OOP loads (i.e., specimens *F.00, FB.00*, and *RBB.00*). It is worth noting that the specimens tested until a definitely higher IP drift level of 1.2% (except for the anomalous *FB.12* specimen), experienced an only slightly higher OOP strength degradation (39%) compared with the previous. It thus seems that the most relevant strength degradation occurs at low IP drift values (until 0.5%), consistently with the fact that all masonry infill walls reached their IP maximum capacity for a drift level between 0.2% and 0.3%, with consequent damage propagation and strength degradation.

Fig. 23 shows the experimental results of the combined IP/OOP tests plotting the OOP strength reduction of all specimens versus the previously attained IP drift level. These values represent the ratio between the OOP strength of each FRM/TRM solution and its corresponding value obtained on the undamaged wall. In the same chart, the OOP strength degradation values of other experimental tests available in literature are summarized (i.e., Angel et al. 1994; Calvi and Bolognini 2001; Furtado et al. 2016; Ricci et al. 2018). Only tests on unreinforced thin clay masonry infill walls are reported. The latter show a significative OOP strength degradation caused by the previous IP damage and, starting from a drift level of 0.4%, they show, in general, a strength degradation about 73%, which is twice than that of the strengthened panels tested in our research.

According to Verlato et al. (2014), an OOP strength reduction factor $\beta_{a,exp}$, expressing the reduction of masonry strength as a

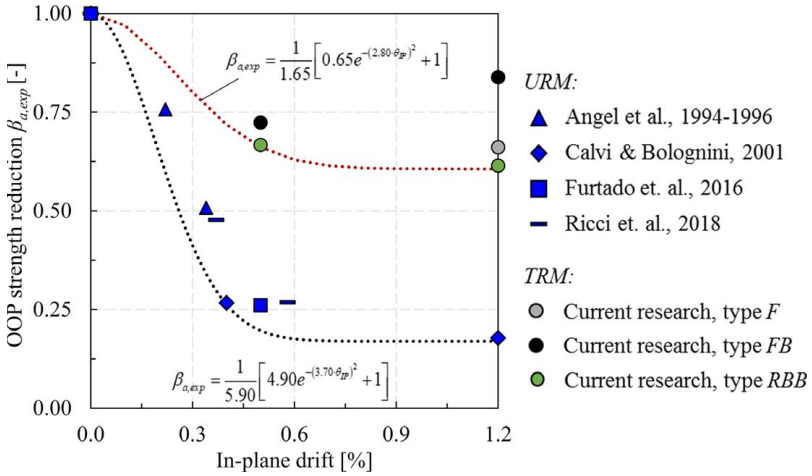

Fig. 23. Out-of-plane strength degradation due to in-plane damage.

function of the in-plane drift θ_{IP}, has been proposed:

$$\beta_{a,\exp} = \frac{1}{a}[(a-1)e^{-(b\cdot\theta_{IP})^2} + 1] \quad (1)$$

where $a = 1.65$ and $b = 2.80$. The reduction factor can be proposed also for URM infill walls assuming $a = 5.90$ and $b = 3.70$. This result can be useful for design approaches that require the OOP verification of the infill wall, which should be related to actual properties of the masonry walls, accounting for the eventual property degradation due to the occurrence of in-plane damage.

In this study, the effect of infill wall openings, such as windows and doors, was not evaluated. The shape and size of these openings clearly affects the overall IP behavior of infilled frames, reducing strength, stiffness, and dissipative capacity, as shown for example by Kakaletsis and Karayannis (2008, 2009) (testing 1/3-scale, one-bay, one-story RC frames infilled with weak or strong URM panels) and by Verlato et al. (2016) (testing full-scale, one-bay, one-story RC frames infilled with strong and ductile URM panels, with deformable joints). Instead, as regards the OOP behavior of the infill walls, it is reasonable to assume, in the hypothesis of a vertical arch or vertical bending resistant mechanism, that this behavior is not significantly affected by the presence of openings, i.e., that the OOP capacity per unit of length of infill wall remains substantially unchanged. However, the presence of openings induces greater IP damage on the infill walls which, in turn, influences their OOP resistance, thus requiring a different calibration of Eq. (1) (as shown by Verlato et al. 2014 with IP/OOP tests of full-scale, one-bay, one-story RC frames infilled with strong unreinforced and reinforced masonry panels). In this framework, it is very likely that the proposed strengthening solutions increase in a fairly proportional way the OOP performance of the infill walls even when there are openings, as these solutions, besides increasing the OOP resistance, significantly limit the capacity reduction due to IP damage.

Non-Structural Elements Design Formulations

The ultimate limit state (ULS) verification of nonstructural elements is satisfied when the OOP capacity is greater than the seismic demand corresponding to the considered design limit state. The

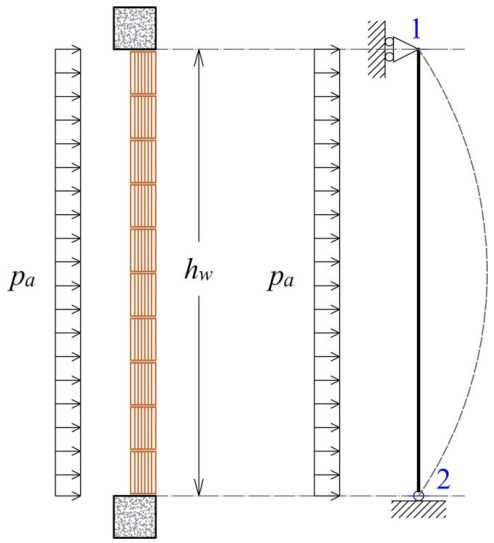

Fig. 24. Distribution of seismic forces.

horizontal seismic force F_a acting on a masonry infill wall is given by

$$F_a = \frac{S_a W_a}{q_a} \quad (2)$$

where F_a = seismic force acting in the center of mass of the nonstructural element, resulting from the distributed forces proportional to mass, W_a = weight of the wall, and S_a = maximum OOP acceleration, which can be calculated, according to Circ. 2019 no. 7 (MIT 2019), by means of response spectra or through simplified formulations of proven validity. The behavior factor q_a can be assumed equal to two (veneer walls, internal partitions, infill walls, etc.), according to Circ. 2019 no. 7 (MIT 2019). As shown in Fig. 24, the OOP seismic action can be represented as a pressure p_a due to the horizontal force F_a distributed along the free height of the wall h_w.

For practical design purposes, it is important to propose and validate adequate formulations for the calculation of the OOP capacity of masonry infill walls; in our case, in particular, for the various strengthening solutions proposed by this research. It is noteworthy that the current EN 1998-1 (CEN 2004) and Italian DM 2018 (MIT

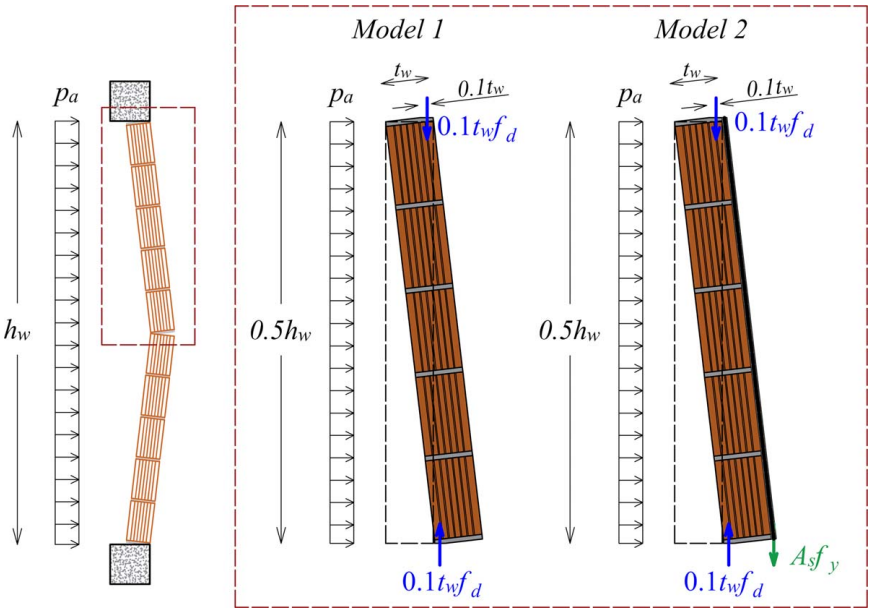

Fig. 25. Out-of-plane capacity models (1 and 2).

2018) do not provide specific recommendations for the calculation of the infill out-of-plane capacity at all. In the case of unreinforced masonry infill walls, it is possible to adopt pure flexural models, as well as to evaluate the out-of-plane bending capacity, taking into account the infill wall self-weight at the section to be verified. Nevertheless, one of the most consistent way to evaluate the OOP infill wall capacity, relies on the model of wall arching between supports, proposed in EN 1996-1-1 (CEN 2005). Starting from these considerations, five models are described and compared in the following subsections, which are: the arch model (*Model 1*), the modified-arch models according to Hak et al. (2013) (*Model 2*) and to FEMA-306 1999 (*Model 3*), the flexural model of the reinforced section (*Model 4*), and the flexural model with simplified vertical load contribution (*Model 5*).

Model 1: Out-of-Plane Arching Mechanism

The ULS verification of masonry infill panels can be carried out assuming that a horizontal or vertical arch develops within the wall thickness. As demonstrated by Angel et al. (1994), it is possible to rely on this mechanism when the masonry panel is built in adherence to the structural elements. The resulting arching mechanism depends on the slenderness ratio of the wall $\lambda = h_w/t_w$ and on the masonry compressive strength f_{md}. The analytical model is based on a simplified configuration of a three-hinged arch with an arch support footprint at the extremities and on the central hinge equal to 0.1 times the thickness of the wall t_w, as shown in Fig. 25. Assuming that the deflection of the arch under the lateral loads may be neglected, the masonry wall resistant moment $M_{r,a}$ can be calculated as

$$M_{r,a} = 0.9 \cdot t_w \cdot f_{md} \cdot 0.1 \cdot t_w = 0.09 \cdot f_{md} \cdot t_w^2 \tag{3}$$

The lateral capacity $q_{\text{lat},d}$ of the infill panel can be derived by assuming the resistant moment equal to the acting moment, i.e., $M_{r,a} = M_s = q_{\text{lat},d} \cdot h_w^2/8$, which leads to

$$q_{\text{lat},d} = 0.72 \cdot f_{md} \left(\frac{t_w}{h_w}\right)^2 \tag{4}$$

To satisfy the ULS verification, the design lateral resistance $q_{\text{lat},d}$ must be higher than the seismic lateral load. The lateral capacity formulation provided by EN 1996-1-1 (CEN 2005) assumes a unitary factor, instead of 0.72 as in Eq. (4), entailing an overestimation of the lateral capacity of about 50%. Considering the type of masonry infills addressed in this research, it seems more reliable to apply the formulation of Eq. (4), which is derived from pure mechanical considerations, also according to Drysdale et al. (1999). In the following, the arching mechanism will be identified as *Model 1*.

Model 2: Arching Mechanism with Simplified Reinforcement Contribution

The formulation provided by *Model 1* does not consider the contribution given by an external reinforcement to the lateral OOP capacity. Hak et al. (2013) proposed a formulation which allow to calculate the OOP capacity of strengthened thin masonry infill walls by adding the contribution of the external reinforcement $M_{r,r}$ to the resistant moment due to the arching mechanism $M_{r,a}$. The approach is based on the simplified assumption that the neutral axis depth can be assumed equal to that used for the calculation of the arching mechanism. The reinforcement resisting moment is defined in Eq. (5), where A_r and f_{yd} are, respectively, the cross-section area and the design yield strength of the vertical reinforcement:

$$M_{r,r} = 0.9 \cdot t_w \cdot A_r \cdot f_{yd} \tag{5}$$

Expressing the resistant moment in terms of equivalent lateral pressure per unit length of the wall L_w, the design lateral resistance can be calculated as

$$q_{\text{lat},d} = 0.72 \cdot f_{md} \left(\frac{t_w}{h_w}\right)^2 + 7.2 \frac{t_w}{L_w h_w^2} A_r f_{yd} \tag{6}$$

Model 3: Modified-Arch Model According to FEMA-306

According to FEMA-306 (FEMA 1999, chapter 8), the uniform pressure causing the infill wall OOP failure can be estimated as

$$q_{\text{lat},d} = 2 \cdot f_{md}\left(\frac{t_w}{h_w}\right)\rho R_1 R_2 \tag{7}$$

where ρ = slenderness parameter dependent on the h_w/t_w ratio and defined in Table 8-5 of the FEMA-306, and R_1 and R_2 = OOP strength reduction factors that take into account, respectively, the existing IP damage and the confining frame flexibility (for further details, please refer to FEMA 1999). In particular, for the purposes of comparison with the experimental case studies, the values adopted are: $\rho = 0.027$ ($h_w/t_w = 17.7$), $R_1 = 1$ and $R_2 = 1$.

Model 4: Out-of-Plane Flexural Mechanism

According to DM 2018 (MIT 2018) and CNR-DT 200 (CNR 2004), the OOP flexural capacity of a reinforced masonry section can be calculated by assuming a compressed stress block with a height equal to αf_{md} and a depth of βx, where $\alpha = 1.00$ (0.85 for design), $\beta = 0.80$ and x is the depth of the neutral axis (see Fig. 26). The section failure may occur on the masonry side, exceeding the ultimate deformation ε_{mu}, as well as on the reinforcement side, exceeding the ultimate deformation ε_{rd}.

In the case of compressive failure of masonry, the resultants of compression forces on the masonry (R_c) and tensile stresses on the reinforcement (R_t) are given by Eqs. (8) and (9), where E_r and A_r = the Young modulus and the equivalent area of the reinforcement, respectively:

$$R_c(x) = \alpha\beta f_{md} L_w x \tag{8}$$

$$R_t(x) = \varepsilon_{mu}\frac{d-x}{x} E_r A_r \tag{9}$$

The position of the neutral axis is determined imposing the equilibrium of the section against vertical translations ($R_c = R_t + N_{Sd}$) as

$$x(N_{Sd}) = \frac{N_{Sd} - E_r A_r \varepsilon_{mu} + \sqrt{(E_r A_r \varepsilon_{mu} - N_{Sd})^2 + 4\alpha\beta f_{md} L_w E_r A_r \varepsilon_{mu} d}}{2\alpha\beta f_{md} L_w} \tag{10}$$

Therefore, assuming $N_{Sd} = 0$, the resisting moment is defined as

$$M_{r,c} = \frac{\alpha\beta f_{md} L_w x}{2}(t_w - \beta x) + \frac{\varepsilon_{mu}}{x}(d-x) E_r A_r \left(d - \frac{t_w}{2}\right) \tag{11}$$

which is correct when the condition $\varepsilon_r \le \varepsilon_{rd}$ is respected.

In the case of tensile failure of reinforcement, the resultant of compression forces on the masonry (R_c) is the same as described in Eq. (8), whereas the resultant of tensile stresses on the reinforcement

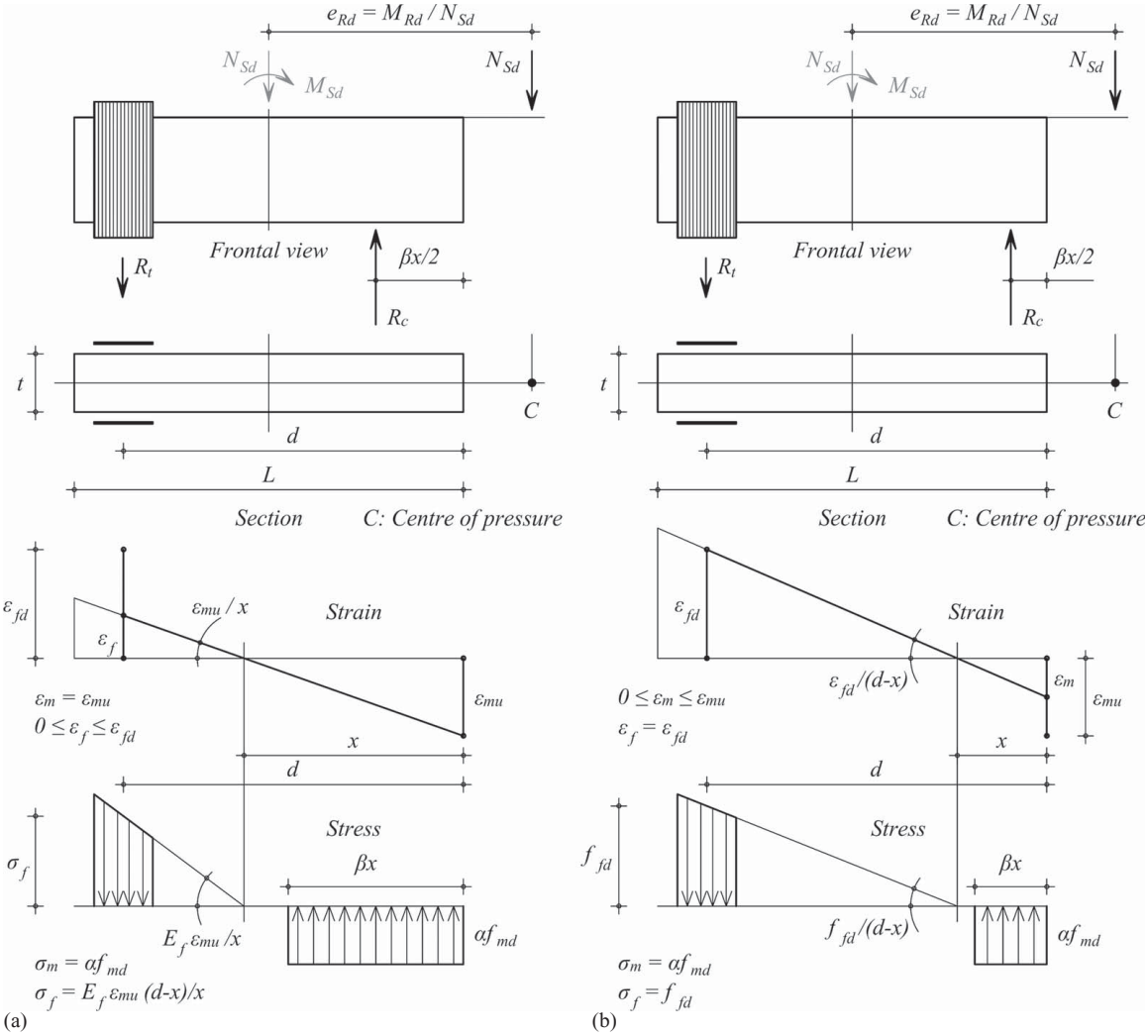

Fig. 26. Cross-section failure mode: (a) compressive failure of masonry; and (b) tensile failure of reinforcement.

J. Compos. Constr., 2020, 24(6): 04020059

(R_t) is given by

$$R_t(x) = \varepsilon_{rd} E_r A_r \tag{12}$$

The position of the neutral axis is determined imposing the equilibrium of the section against vertical translations ($R_c = R_t + N_{Sd}$) as

$$x(N_{Sd}) = \frac{N_{Sd} + E_r A_r \varepsilon_{rd}}{\alpha\beta f_{md} L_w} \tag{13}$$

Therefore, assuming $N_{Sd} = 0$, the resisting moment is defined by

$$M_{r,t} = \frac{\alpha\beta f_{md} L_w x}{2}(t_w - \beta x) + \varepsilon_{rd} E_r A_r \left(d - \frac{t_w}{2}\right) \tag{14}$$

which is correct when the condition $0 \le \varepsilon_m \le \varepsilon_{mu}$ is respected.

The flexural capacity can be taken as the lesser of the above calculated values as

$$M_r = \min\{M_{r,c};\, M_{r,t}\} \tag{15}$$

Expressing the resistant moment in terms of equivalent lateral pressure per unit length of the wall L_w, the design lateral resistance can be calculated by

$$q_{\text{lat},d} = \frac{8M_r}{L_w h_w^2} \tag{16}$$

Model 5: Out-of-Plane Flexural Mechanism with Simplified Vertical Load Contribution

The formulation provided by *Model 4* does not consider the contribution given by the relevant vertical load that, in the case of infill walls built in adherence to the structural elements, develops within the masonry thickness as soon as the wall deflects out of its plane, due to the action of lateral loads and boundary conditions. Neglecting the vertical load, or taking into account a value of vertical load equal to the infill wall self-weight at the section to be verified, may bring to excessive underestimation of this contribution that, in turn, means excessively conservative estimations of the OOP infill wall capacity.

To take into account the actual vertical load acting at the wall mid-height section, a rigorous procedure would require an iterative calculation. However, a simplified procedure for design purpose can assume that the vertical load acting on the mid-height section is evaluated according to the arching mechanism (as given by *Model 1*), adding the self-weight of the wall acting on such section. The position of the neutral axis of *Model 4* can be then evaluated on the basis of this value of vertical load and, as a consequence, the values of resisting moment and flexural capacity of the wall in presence of a vertical load can be calculated. Conceptually, *Model 5* is not much different from *Model 2*, although the results of *Model 5* are affected by the relative quantities of masonry and reinforcement which influence the position of the neutral axis.

Validation of the Proposed Formulations

The proposed formulations were implemented and validated on the experimental results of tested strengthened masonry infills (i.e., *F*, *FB* and *RBB*), in case of undamaged masonry. The results are summarized in Fig. 27. All calculations were carried out considering the mean mechanical values of the materials, i.e., neglecting partial safety factors. Furthermore, the calculated values of lateral resistance, consistently with the experimental conditions, were obtained by evaluating the out-of-plane thrust applied along four horizontal load lines. In the case of plaster type *F*, the area and the yield strength of the reinforcement are considered to be, respectively, the cross section and the tensile strength of the external plaster layer.

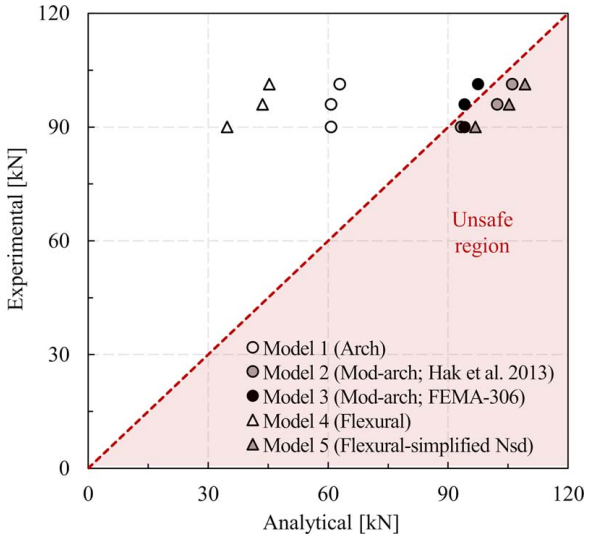

Fig. 27. OOP lateral capacity: comparison between experimental and analytical values.

As expected, *Model 1* underestimates the experimental lateral capacity (with 33–38% deviation) since it neglects the contribution of the reinforcement layer. On the other hand, *Model 2*, although implementing a simplified evaluation of the reinforcement contribution to the masonry wall capacity, gives results that are very close to the experimental ones (with 4–7% overestimation). *Model 3*, i.e., the modified-arch model of FEMA-306 (FEMA 1999), provides the closest results (with ±4% deviation); however, considering that it does not specifically take into account the contribution of the reinforcement layer (as for *Model 1*), it could be non-conservative when applied to typical weak masonry infill walls made of hollow clay units, such as the URM infill walls of our research.

Model 4, neglecting the contribution of the vertical load acting on the section, significantly underestimate the experimental lateral capacity (with 55–61% deviation). Conversely, *Model 5*, which takes this contribution into account, albeit in a simplified way, provides better results than *Model 4*, with an overestimation of the experimental results of about 8%–10%, i.e., slightly higher than that of *Model 2* despite the more detailed evaluation of the neutral axis in *Model 5*.

Conclusions

Considering the results of IP tests, it can be concluded that:

- All specimens, although strengthened with various solutions, reached the peak strength at low drift levels (0.2%–0.3%). These outcomes are compatible with other results found in the literature, for thin clay masonry infill walls. These results confirm that, particularly in the case of masonry infill walls made with weak fragile clay units, the inter-story drift values proposed by EN1998 for the damage limit state ($\theta = 0.5\%$), should be regarded as values to be found from analyses on bare frames, and should be carefully taken into account.
- In general, IP capacity and stiffness of thin and weak clay masonry infill walls increase with the use of fiber-reinforced plasters of high mechanical properties. However, the use of a glass

fiber plaster alone (*F*), cannot significantly reduce the damage due to IP displacements.

- Embedding a strengthening mesh on the external plaster layers produces a confinement effect, which reduces IP damage of the infill wall. The basalt mesh cannot prevent crushing of masonry units and detachment of little plaster portions, nevertheless it has an evident beneficial effect in preventing the expulsion of masonry and plaster portions. The mesh also allows controlling the initial post-peak branch and obtaining higher values of equivalent viscous damping and energy dissipation capacity (despite damage reduction).
- The previous mesh effects are irrespective of the quality of the plaster, as they also occur in specimens (*RBB*) with low-quality plaster, simulating the effect of a preexisting material.
- When taking into account the behavior of URM infill walls, all of the previous considerations are confirmed. Indeed, at the end of the IP test, the URM specimen showed a significative damage distribution compared with the specimens of this research, especially along the infill–frame interface. In addition, compared with the URM specimen, the strengthening solutions allowed an increase in strength (F_{max} and therefore F_{ult}) of about 30% (*F*) or 50% (*FB*) and an increase in deformation capacity, in terms of θ_{Fult}, of about 50% (*RBB*) or 70% (*F*, *FB*); the initial stiffness K_{max} was also increased by about 15% (*RBB*, *F*) or 50% (*FB*).

Considering the results of the OOP tests, it can be concluded that:

- The comparison among strengthened infills and the reference unreinforced one showed a relevant increase of the OOP strength in the first case. Indeed, all the strengthened specimens, after reaching an IP drift of 1.2%, showed an OOP capacity at least 26% higher than that of the reference unreinforced specimen.
- Although the final values of OOP capacity, at each IP drift level, do not differ significantly, it was possible to notice that the use of an embedded mesh, in *FB* and *RBB* solutions, improved the OOP response of the infill wall, preventing its possible brittle collapse. Conversely, also taking into account the actual dynamic behavior, type *F* strengthening could yield to a more fragile collapse.
- The use of anchorage bars embedded into the plaster layer and fixed to the upper beam (*RBB* specimens), although not significantly influencing the OOP capacity of the infill, allowed better control of the OOP failure mode after the peak strength. This addresses at a combined solution (mesh + anchorage bars) as particularly promising for controlling the masonry infill wall OOP behavior.
- The experimental tests allowed evaluation of the reduction of OOP capacity due to IP damage. The strength degradation is around 39% at 1.2% drift, and it seems to be already stabilized after an initial relevant strength degradation of 33% at 0.5% drift. The definitely higher strength degradation values (i.e., 73% at 1.2% drift) of similar URM walls further demonstrate the effectiveness of the proposed strengthening solutions.

Lastly, some analytical models for the calculation of the OOP capacity of masonry infill walls were described and validated on the experimental results of IP undamaged panels:

- As expected, both the arching (*Model 1*) and the out-of-plane flexural (*Model 4*) mechanisms significantly underestimate the OOP infill wall capacity, with a reduction up to 61% compared with the experimental values.
- Other hybrid formulations which account for, in a simplified way, the contribution of the external reinforcement (*Model 2*) and the contribution of the vertical load acting at wall mid-height (*Model 5*), provide more realistic values of the lateral capacity and can be proposed as reliable formulations for design/verification purposes. In particular, both *Model 2* and *Model 5* only slightly overestimate the experimental results, with deviations of up to 7% and 10%, respectively.
- Finally, the arch-modified model proposed in FEMA-306 (FEMA 1999; *Model 5*) provides the lateral capacity values that best approximate the experimental ones. However, it does not explicitly take into account the effect of external reinforcement, therefore it seems that the models reported in the previous point could be more suitable for the scope of evaluating thin masonry infill walls strengthened with various types of externally applied systems.

Data Availability Statement

Some or all data, models, or code that support the findings of this study are available from the corresponding author upon reasonable request.

Acknowledgments

This research activity was funded by Kerakoll S.p.A. This study has been also partly supported by a program funded by the Presidency of the Council of Ministers Department of Civil Protection (2019–2021 DPC- ReLUIS). The experimental tests were carried out at the Laboratory of Structural Materials Testing of the University of Padova, Italy.

(All photos: University of Padova and Kerakoll S.p.A., Italy.)

Notation

The following notation symbols are used in this paper:

A_r = cross-section area of infill wall reinforcement;
a_{eq} = equivalent seismic acceleration;
d = effective depth of reinforcement;
E_r = Young modulus of reinforcement;
F_a = horizontal seismic force acting on a masonry infill;
F_{max} = maximum resistance of infill wall;
F_{ult} = ultimate resistance of infill wall, corresponding to resistance degradation of 20%;
f_{md} = design compressive strength of masonry;
f_{yd} = design tensile strength of reinforcement;
h_w = height of infill wall;
L_w = length of infill wall;
M_r = flexural capacity of infill wall;
$M_{r,a}$ = bending moment, calculated per unit length, due to arching mechanism;
$M_{r,c}$ = flexural capacity of the infill wall due to compressive failure of masonry;
$M_{r,r}$ = bending moment, calculated per unit length, due to tensile strength of reinforcement;
$M_{r,t}$ = flexural capacity of the infill wall due to tensile reinforcement failure;
M_s = calculated acting moment per unit length of infill wall;
N_{Sd} = vertical load acting on the wall;
p_a = seismic pressure acting on infill wall surface;
q_a = behavior factor of infill wall;
$q_{lat,d}$ = design lateral strength, expressed as a uniform load distributed over the wall length;
R_c = resultant of compression forces on masonry;
R_t = resultant of tensile stresses on reinforcement;
R_1 = out-of-plane strength reduction factor taking into account the in-plane damage of infill;

R_2 = out-of-plane strength reduction factor taking into account the confining frame flexibility;
S = soil amplification factor;
S_a = maximum out-of-plane acceleration acting on the infill wall;
T_a = fundamental vibration period of the infill wall in the out-of-plane direction;
T_1 = fundamental vibration period of the building in the considered direction;
t_w = thickness of infill wall;
W_a = weight of infill wall;
x = depth of neutral axis;
α = reduction coefficient to take into account long-term effects on the compressive strength;
β = coefficient to calculate the depth of the stress block;
$\beta_{a,\text{exp}}$ = masonry strength reduction factor, function of the in-plane drift;
δ = out-of-plane displacement;
$\delta_{F\text{max}}$ = out-of-plane displacement at the maximum out-of-plane strength;
ε_{mu} = ultimate deformation of masonry;
ε_{rd} = ultimate deformation of reinforcement;
θ = in-plane inter-story drift ratio;
$\theta_{F\text{max}}$ = inter-story drift ratio at maximum resistance;
$\theta_{F\text{ult}}$ = inter-story drift ratio at ultimate resistance;
θ_{IP} = maximum level of in-plane drift ratio applied to the specimen;
λ = slenderness ratio of infill wall; and
ρ = slenderness parameter of infill wall.

References

Angel, R. E., D. P. Abrams, D. Shapiro, J. Uzarski, and M. Webster. 1994. *Behavior of reinforced concrete frames with masonry infills*. Technical Report. Champaign, IL: Univ. of Illinois at Urbana-Champaign.

Anil, Ö, and S. Altin. 2007. "An experimental study on reinforced concrete partially infilled frames." *Eng. Struct.* 29 (3): 449–460. https://doi.org/10.1016/j.engstruct.2006.05.011.

Baio Dias, A., F. da Porto, E. Fehling, P. B. Lourenço, P. Morandi, E. Vintzileou, and A. Yakut. 2014. "Innovative systems for earthquake resistant masonry enclosures in RC buildings." In *Proc., 9th Int. Masonry Conf.*, 1–12. Minho, Portugal: University of Minho and ISISE and International Masonry Society (IMS).

Bazzurro, P., et al. 2009. *Learning from earthquakes: The Mw 6.3 Abruzzo, Italy, Earthquake of April 6, 2009*. EERI Special Earthquake Report. Oakland, CA: Earthquake Engineering Research Institute.

Bergami, A. V., and C. Nuti. 2015. "Experimental tests and global modeling of masonry infilled frames." *Earthquakes Struct.* 9 (2): 281–303. https://doi.org/10.12989/eas.2015.9.2.281.

Blackard, B., K. Willam, and M. Sivaselvan. 2009. *Experimental observations of masonry infilled reinforced concrete frames with openings*, 199–221. ACI Special Publication 265. Farmington Hills, MI: American Concrete Institute.

Braga, F., V. Manfredi, A. Masi, A. Salvatori, and M. Vona. 2011. "Performance of non-structural elements in RC buildings during the L'Aquila, 2009 earthquake." *Bull. Earthquake Eng.* 9 (1): 307–324. https://doi.org/10.1007/s10518-010-9205-7.

Calvi, G. M., and D. Bolognini. 2001. "Seismic response of reinforced concrete frames infilled with weakly reinforced masonry panels." *J. Earthquake Eng.* 5 (2): 153–185. https://doi.org/10.1080/13632460109350390.

CEN (European Committee for Standardization). 1998a. *Methods of test for mortar for masonry, Part 1: determination of particle size distribution (by sieve analysis)*. EN 1015-1. Brussels, Belgium: CEN.

CEN (European Committee for Standardization). 1998b. *Methods of test for masonry, Part 1: Determination of compressive strength*. EN 1052-1. Brussels, Belgium: CEN.

CEN (European Committee for Standardization). 1999. *Methods of test for masonry, Part 2: Determination of flexural strength*. EN 1052-2. Brussels, Belgium: CEN.

CEN (European Committee for Standardization). 2004. *Design of structures for earthquake resistance, Part 1: General rules, seismic actions and rules for buildings*. Eurocode 8, EN 1998-1. Brussels, Belgium: CEN.

CEN (European Committee for Standardization). 2005. *Design of masonry structures, Part 1-1: General rules for reinforced and unreinforced masonry structures*. Eurocode 6, EN 1996-1-1. Brussels, Belgium: CEN.

CEN (European Committee for Standardization). 2006a. *Methods of test for mortar for masonry—Determination of flexural and compressive strength of hardened mortar*. EN 1015-11/A1. Brussels, Belgium: CEN.

CEN (European Committee for Standardization). 2006b. *Products and systems for the protection and repair of concrete structures—Test methods—Determination of modulus of elasticity in compression*. EN 13412. Brussels, Belgium: CEN.

CEN (European Committee for Standardization). 2013. *Testing hardened concrete, Part 13: Determination of secant modulus of elasticity in compression*. EN 12390-13. Brussels, Belgium: CEN.

CEN (European Committee for Standardization). 2015. *Specification for masonry units, Part 1: Clay masonry units*. EN 771-1. Brussels, Belgium: CEN.

CEN (European Committee for Standardization). 2016a. *Specification for mortar for masonry, Part 1: Rendering and plastering mortar*. EN 998-1. Brussels, Belgium: CEN.

CEN (European Committee for Standardization). 2016b. *Specification for mortar for masonry, Part 2: Masonry mortar*. EN 998-2. Brussels, Belgium: CEN.

Chiozzi, A., and E. Miranda. 2017. "Fragility functions for masonry infill walls with in-plane loading." *Earthquake Eng. Struct. Dyn.* 46 (15): 2831–2850. https://doi.org/10.1002/eqe.2934.

CNR (National Research Council). 2004. *Guide for the design and construction of externally bonded FRP systems for strengthening existing structures*. [In Italian.] CNR-DT 200. Rome: CNR.

Crisafulli, F. J. 1997. "Seismic behaviour of reinforced concrete structures with masonry infills." Ph.D. thesis, Civil Engineering, Univ. of Canterbury.

da Porto, F., G. Guidi, M. Dalla Benetta, and N. Verlato. 2013. "Combined in-plane/out-of-plane experimental behaviour of reinforced and strengthened infill masonry walls." In *Proc., 12th Canadian Masonry Symp*. Vancouver, BC: Canadian Masonry Symposium (CMS).

da Porto, F., G. Guidi, N. Verlato, and C. Modena. 2015. "Effectiveness of plasters and textile reinforced mortars for strengthening clay masonry infill walls subjected to combined in-plane/out-of-plane actions"" [Wirksamkeit von Putz und textilbewehrtem Mörtel bei der Verstärkung von Ausfachungswänden aus Ziegel]. *Mauerwerk* 19 (5): 334–354. https://doi.org/10.1002/dama.201500673.

da Porto, F., N. Verlato, G. Guidi, and C. Modena. 2016. "The INSYSME project : Innovative construction systems for earthquake resistant masonry infill walls." In *Vol. 6 of Proc., 16th Int. Brick and Block Masonry—Trends, Innovations and Challenges Conf.*, edited by C. Modena, F. da Porto, and M. R. Valluzzi, 1173–1178. London: Taylor & Francis Group.

Dafnis, A., H. Kolsch, and H. G. Reimerdes. 2002. "Arching in masonry walls subjected to earthquake motions." *J. Struct. Eng.* 128 (2): 153–159. https://doi.org/10.1061/(ASCE)0733-9445(2002)128:2(153).

Dawe, J. L., and C. K. Seah. 1989. "Behaviour of masonry infilled steel frames." *Can. J. Civ. Eng.* 16 (6): 865–876. https://doi.org/10.1139/l89-129.

De Luca, F., G. M. Verderame, A. Pérez-garcía, and F. Gómez-martínez. 2014. "The structural role played by masonry infills on RC building performances after the 2011 Lorca, Spain, earthquake." *Bull. Earthquake Eng.* 12 (5): 1999–2026. https://doi.org/10.1007/s10518-013-9500-1.

De Martino, G., M. Di Ludovico, A. Prota, C. Moroni, G. Manfredi, and M. Dolce. 2017. "Estimation of repair costs for RC and masonry residential buildings based on damage data collected by post-earthquake visual inspection." *Bull. Earthquake Eng.* 15 (4): 1681–1706. https://doi.org/10.1007/s10518-016-0039-9.

De Risi, M. T., A. Furtado, H. Rodrigues, J. Melo, G. M. Verderame, A. Arêde, H. Varum, and G. Manfredi. 2019. "Experimental analysis of textile reinforced mortars strengthening strategies against the out-of-plane collapse of masonry infill walls." In *Proc., 18th CONVEGNO ANIDIS*, SG13–57. Pisa, Italy: Pisa University Press srl.

De Risi, R., A. Sextos, P. Zimmaro, A. Simonelli, and J. P. Stewart. 2018. "The 2016 central Italy earthquake sequence: Observations of incremental building damage." In *Proc., 11th U.S. National Conf. on Earthquake Engineering*. Los Angeles, California: Earthquake Engineering Research Institute (EERI).

Di Ludovico, M., A. Prota, C. Moroni, G. Manfredi, and M. Dolce. 2017a. "Reconstruction process of damaged residential buildings outside historical centres after the L'Aquila earthquake: Part I—"light damage" reconstruction." *Bull. Earthquake Eng.* 15 (2): 667–692. https://doi.org/10.1007/s10518-016-9877-8.

Di Ludovico, M., A. Prota, C. Moroni, G. Manfredi, and M. Dolce. 2017b. "Reconstruction process of damaged residential buildings outside historical centres after the L'Aquila earthquake: Part II—"heavy damage" reconstruction." *Bull. Earthquake Eng.* 15 (2): 693–729. https://doi.org/10.1007/s10518-016-9979-3.

Doğangün, A., A. Ural, H. Sezen, Y. Güney, and F. K. Fırat. 2013. "The 2011 earthquake in Simav, Turkey and seismic damage to reinforced concrete buildings." *Buildings* 3 (1): 173–190. https://doi.org/10.3390/buildings3010173.

Dolce, M., and A. Goretti. 2015. "Building damage assessment after the 2009 Abruzzi earthquake." *Bull. Earthquake Eng.* 13 (8): 2241–2264. https://doi.org/10.1007/s10518-015-9723-4.

Donà, M., M. Minotto, E. Bernardi, E. Saler, N. Verlato, and F. da Porto. 2019. "Macro-modelling of combined in-plane and out-of-plane seismic response of thin strengthened masonry infills." In *Proc., 7th Int. Conf. on Computational Methods in Structural Dynamics and Earthquake Engineering*, 2449–2463. Athens, Greece: Institute of Structural Analysis and Antiseismic Research School of Civil Engineering, National Technical University of Athens (NTUA).

Donà, M., M. Minotto, E. Saler, G. Tecchio, and F. da Porto. 2017. "Combined in-plane and out-of-plane seismic effects on masonry infills in RC frames." *Int. J. Earthquake Eng.* 34: 157–173.

Drysdale, R. G., and A. S. Essawy. 1988. "Out-of-Plane bending of concrete block walls." *J. Struct. Eng.* 114 (1): 121–133. https://doi.org/10.1061/(ASCE)0733-9445(1988)114:1(121).

Drysdale, R. G., A. A. Hamid, and L. R. Baker. 1999. *Masonry structures: Behaviour and design*. Boulder, CO: Prentice Hall.

El-Dakhakhni, W. W., A. A. Hamid, Z. H. R. Hakam, and M. Elgaaly. 2006. "Hazard mitigation and strengthening of unreinforced masonry walls using composites." *Compos. Struct.* 73 (4): 458–477. https://doi.org/10.1016/j.compstruct.2005.02.017.

FEMA. 1999. "Evaluation of earthquake damaged concrete and masonry wall buildings—Basic procedures manual." Chap. 8 in *Infilled frames*, 183–214. FEMA-306. Washington, DC: FEMA.

Fiorato, A. E., M. A. Sozen, and W. L. Gamble. 1970. *An investigation of the interaction of RC frames with masonry filler walls*. Technical Report. Champaign, IL: Univ. of Illinois at Urbana-Champaign.

Flanagan, R. D., and R. M. Bennett. 1999. "Bidirectional behavior of structural clay tile infilled frames." *J. Struct. Eng.* 125 (3): 236–244. https://doi.org/10.1061/(ASCE)0733-9445(1999)125:3(236).

Fragomeli, A., et al. 2017. "Performance of masonry buildings in the seismic sequence of Central Italy 2016—Part 1 : Overview." *Progettazione Sismica* 8 (2): 49–77.

Furtado, A., H. Rodrigues, A. Arêde, and H. Varum. 2016. "Experimental evaluation of out-of-plane capacity of masonry infill walls." *Eng. Struct.* 111: 48–63. https://doi.org/10.1016/j.engstruct.2015.12.013.

Gazic, G., and V. Sigmund. 2016. "Cyclic testing of single-span weak frames with masonry infill." *J. Croatian Assoc. Civ. Eng.* 68 (8): 617–633. https://doi.org/10.14256/JCE.1614.2016.

Hak, S., P. Morandi, and G. Magenes. 2013. *Damage control of masonry. Infills in seismic design*. Pavia, Italy: IUSS.

Hermanns, L., A. Fraile, E. Alarcón, and R. Álvarez. 2014. "Performance of buildings with masonry infill walls during the 2011 Lorca earthquake." *Bull. Earthquake Eng.* 12 (5): 1977–1997. https://doi.org/10.1007/s10518-013-9499-3.

Holmes, M. 1961. "Steel frames with brickwork and concrete infilling." *Proc. Inst. Civ. Eng.* 19 (4): 473–478. https://doi.org/10.1680/iicep.1961.11305.

INSYSME. 2014. *Report on types of structural frames, related enclosure wall systems, and requirements for the construction systems*. INSYSME Project D3.1. Padova, Italy: INSYSME.

Ismail, N., T. El-Maaddawy, N. Khattak, K. Q. Walsh, and J. M. Ingham. 2018. "Out-of-plane behaviour of in-plane damaged masonry infills strengthened using fibre reinforced matrix." In *Proc., Int. Masonry Society Conf.*, 2200–2216. Milan, Italy: International Masonry Society (IMS) and Technical University of Milan.

Kakaletsis, D. J., K. N. David, and C. G. Karayannis. 2011. "Effectiveness of some conventional seismic retrofitting techniques for bare and infilled R/C frames." *Struct. Eng. Mech.* 39 (4): 499–520. https://doi.org/10.12989/sem.2011.39.4.499.

Kakaletsis, D. J., and C. G. Karayannis. 2008. "Influence of masonry strength and openings on infilled R/C frames under cycling loading." *J. Earthquake Eng.* 12 (2): 197–221. https://doi.org/10.1080/13632460701299138.

Kakaletsis, D. J., and C. G. Karayannis. 2009. "Experimental investigation of infilled reinforced concrete frames with openings." *ACI Struct. J.* 106 (2): 132–141.

Kalali, A. 2012. "Cyclic behavior of perforated masonry walls strengthened with glass fiber reinforced polymers." *Scientia Iranica* 19 (2): 151–165. https://doi.org/10.1016/j.scient.2012.02.011.

Koutas, L. N., and D. A. Bournas. 2019. "Out-of-plane strengthening of masonry-infilled RC frames with textile-reinforced mortar jackets." *J. Compos. Constr.* 23 (1): 04018079. https://doi.org/10.1061/(ASCE)CC.1943-5614.0000911.

Lunn, D. S., and S. H. Rizkalla. 2011. "Strengthening of infill masonry walls with FRP materials." *J. Compos. Constr.* 15 (2): 206–214. https://doi.org/10.1061/(ASCE)CC.1943-5614.0000088.

Mainstone, R. J. 1971. "On The stiffness and strengths of infilled frames." *Proc. Inst. Civ. Eng.* 49 (2): 57–90. https://doi.org/10.1680/iicep.1971.6267.

Mainstone, R. J., and G. A. Weeks. 1970. "The influence of a bounding frame on the racking stiffness and strengths of brick walls." In *Proc., 2nd Int. Brick Masonry Conf., Building Research Establishment*, 165–171. Stoke-on-Trent, UK: British Ceramic Research Association.

Manos, G., D. Naxakis, and V. Soulis. 2015. "The dynamic and earthquake response of a two story old r/c building with masonry infills in Lixouri-Kefalonia, Greece including soil-foundation deformability." In *Proc., 5th Int. Conf. on Computational Methods in Structural Dynamics and Earthquake Engineering*, 435–459. Athens, Greece: Institute of Structural Analysis and Antiseismic Research School of Civil Engineering, National Technical University of Athens (NTUA).

Marinković, M., and C. Butenweg. 2019. "Innovative decoupling system for the seismic protection of masonry infill walls in reinforced concrete frames." *Eng. Struct.* 197: 109435. https://doi.org/10.1016/j.engstruct.2019.109435.

Martins, A., G. Vasconcelos, R. Fangueiro, and F. Cunha. 2015. "Experimental assessment of an innovative strengthening material for brick masonry infills." *Composites, Part B* 80: 328–342. https://doi.org/10.1016/j.compositesb.2015.06.012.

Masi, A., L. Chiauzzi, G. Santarsiero, M. Liuzzi, and V. Tramutoli. 2017. "Seismic damage recognition based on field survey and remote sensing: General remarks and examples from the 2016 Central Italy earthquake." *Nat. Hazards* 86 (S1): 193–195. https://doi.org/10.1007/s11069-017-2776-8.

Masi, A., L. Chiauzzi, G. Santarsiero, V. Manfredi, S. Biondi, E. Spacone, C. Del Gaudio, P. Ricci, G. Manfredi, and G. M. Verderame. 2019. "Seismic response of RC buildings during the Mw 6.0 August 24, 2016 central Italy earthquake: The amatrice case study." *Bull. Earthquake Eng.* 17 (10): 5631–5654. https://doi.org/10.1007/s10518-017-0277-5.

Mehrabi, A. B., P. Benson Shing, M. P. Schuller, and J. L. Noland. 1996. "Experimental evaluation of masonry-infilled RC frames." *J. Struct. Eng.* 122 (3): 228–237. https://doi.org/10.1061/(ASCE)0733-9445(1996)122:3(228).

Mehrabi, A. B., P. B. Shing, M. P. Schuller, and J. L. Noland. 1994. *Performance of masonry-infilled RIC frames under in-plane lateral loads*. Technical Report. Boulder, CO: Univ. of Colorado at Boulder.

MIT (Ministry of Infrastructure and Transport). 2008. *New technical standards for constructions 2008*. DM 2008/01/14, "S.O. No. 30 alla G.U. del 4 Febbraio 2008, No. 29". [In Italian.] Rome: MIT.

MIT (Ministry of Infrastructure and Transport). 2018. *Update of the "technical standards for constructions" 2018*. DM 2018/01/17, "S.O. No. 8 alla G.U. del 20 Febbraio 2018, No. 32". [In Italian.] Rome: MIT.

MIT (Ministry of Infrastructure and Transport). 2019. *Instructions for the application of the "update of the "technical standards for constructions" 2018"*. Circ. 2019/01/21 no. 7, "S.O. No. 5 alla G.U. del 11 Febbraio 2019, No. 35". [In Italian.] Rome: MIT.

Mohammadi, M., and V. Akrami. 2010. "An engineered infilled frame: Behavior and calibration." *J. Constr. Steel Res.* 66 (6): 842–849. https://doi.org/10.1016/j.jcsr.2010.01.008.

Mohammadi, M., V. Akrami, and R. Mohammadi-Ghazi. 2011. "Methods to improve infilled frame ductility." *J. Struct. Eng.* 137 (6): 646–653. https://doi.org/10.1061/(ASCE)ST.1943-541X.0000322.

Morandi, P., R. R. Milanesi, and G. Magenes. 2018. "Innovative solution for seismic-resistant masonry infills with sliding joints: In-plane experimental performance." *Eng. Struct.* 176: 719–733. https://doi.org/10.1016/j.engstruct.2018.09.018.

Palieraki, V., C. Zeris, E. Vintzileou, and C.-E. Adami. 2018. "In-plane and out-of plane response of currently constructed masonry infills." *Eng. Struct.* 177: 103–116. https://doi.org/10.1016/j.engstruct.2018.09.047.

Papanicolaou, C. G., T. C. Triantafillou, M. Papathanasiou, and K. Karlos. 2007. "Textile reinforced mortar (TRM) versus FRP as strengthening material of URM walls: Out-of-plane cyclic loading." *Mater. Struct.* 41 (1): 143–157. https://doi.org/10.1617/s11527-007-9226-0.

Penna, A., P. Morandi, M. Rota, C. F. Manzini, F. da Porto, and G. Magenes. 2014. "Performance of masonry buildings during the emilia 2012 earthquake." *Bull. Earthquake Eng.* 12 (5): 2255–2273. https://doi.org/10.1007/s10518-013-9496-6.

Pereira, M. F. P., M. F. N. Pereira, J. E. D. Ferreira, and P. B. Lourenço. 2011. "Behavior of masonry infill panels in RC frames subjected to in plane and out of plane loads." In *Proc., 7th Int. Conf. AMCM*. Krakow, Poland: Wydawnictwo Politechniki Krakowskiej im. Tadeusza Kościuszki.

Polyakov, S. V. 1960. "On the interaction between masonry filler walls and enclosing frame when loaded in plane of the wall." In *Translations in Earthquake Engineering*, 36–42. Oakland, CA: Earthquake Engineering Research Institute.

Preti, M., L. Migliorati, and E. Giuriani. 2015. "Experimental testing of engineered masonry infill walls for post-earthquake structural damage control." *Bull. Earthquake Eng.* 13 (7): 2029–2049. https://doi.org/10.1007/s10518-014-9701-2.

Ricci, P., M. Di Domenico, and G. M. Verderame. 2018. "Experimental assessment of the in-plane/out-of-plane interaction in unreinforced masonry infill walls." *Eng. Struct.* 173: 960–978. https://doi.org/10.1016/j.engstruct.2018.07.033.

Ricci, P., F. De Luca, and G. M. Verderame. 2011. "6th April 2009 L'Aquila earthquake, Italy: Reinforced concrete building performance." *Bull. Earthquake Eng.* 9 (1): 285–305. https://doi.org/10.1007/s10518-010-9204-8.

Saatcioglu, M., F. Serrato, and S. Foo. 2005. "Seismic performance of masonry infill walls retrofitted with CFRP sheets." In *Proc., 7th Int. Symp. on Fiber-Reinforced Polymer Reinforcement for Concrete Structures*, 341–354. Farmington Hills, Michigan: American Concrete Institute.

Sagar, S. L., V. Singhal, and D. C. Rai. 2019. "In-plane and out-of-plane behavior of masonry-infilled RC frames strengthened with fabric-reinforced cementitious matrix." *J. Compos. Constr.* 23 (1): 04018073. https://doi.org/10.1061/(ASCE)CC.1943-5614.0000905.

Silva, L. M., G. Vasconcelos, P. B. B. Lourenço, and F. Akhoundi. 2016. "Experimental evaluation of a constructive system for earthquake-resisting masonry enclosure walls." In *Proc., 16th Int. Brick and Block Masonry Conf.*, 1333–1340. Leiden, The Netherlands: Taylor & Francis Group.

Stafford-Smith, B. 1962. "Lateral stiffness of infilled frames." *J. Struct. Div.* 88 (6): 183–226.

Thomas, F. C. 1952. "The strength of brickwork." *J. Struct. Eng.* 31 (2): 35–46.

Tu, Y.-H., T. H. Chuang, P.-M. Liu, and Y. S. Yang. 2010. "Out-of-plane shaking table test on unreinforced masonry panels in RC frame." *Eng. Struct.* 32 (12): 3925–3935. https://doi.org/10.1016/j.engstruct.2010.08.030.

Tumialan, J. G., N. Galati, and A. Nanni. 2003. "Fiber-reinforced polymer strengthening of unreinforced masonry walls subject to out-of-plane loads." *ACI Struct. J.* 100 (3): 321–329.

Valluzzi, M. R., F. da Porto, E. Garbin, and M. Panizza. 2014. "Out-of-plane behaviour of infill masonry panels strengthened with composite materials." *Mater. Struct.* 47 (12): 2131–2145. https://doi.org/10.1617/s11527-014-0384-6.

Vasconcelos, G., S. Abreu, R. Fangueiro, and F. Cunha. 2012. "Retrofitting masonry infill walls with textile reinforced mortar." In *Proc., 15th World Conf. on Earthquake Engineering*. 30588–30597. Red Hook, NY: Curran Associates, Inc.

Verderame, G. M., P. Ricci, F. De Luca, C. Del Gaudio, and M. T. De Risi. 2014. "Damage scenarios for RC buildings during the 2012 Emilia (Italy) earthquake." *Soil Dyn. Earthquake Eng.* 66: 385–400. https://doi.org/10.1016/j.soildyn.2014.06.034.

Verlato, N., G. Guidi, and F. da Porto. 2014. "Calcolo della resistenza fuori piano di tamponature realizzate con il sistema Antiespulsione : Modellazione analitica e proposte progettuali." *Murature Oggi* 116 (3): 8–16.

Verlato, N., G. Guidi, F. da Porto, and C. Modena. 2016. "Innovative systems for masonry infill walls based on the use of deformable joints: Combined in-plane/out-of-plane tests." In *Proc., 16th Int. Brick and Block Masonry Conf.*, 1359–1366. Leiden, The Netherlands: Taylor & Francis Group.

Vicente, R., H. Rodriguez, A. Costa, H. Varum, and J. A. R. Mendes da Silva. 2010. "Masonry enclosure walls: Lessons learnt from the recent Abruzzo Earthquake." In *Proc., 14th European Conf. of Earthquake Engineering*, 1094–1101. Red Hook, NY: Curran Associates, Inc.

Vintzileou, E., C.-E. Adami, and V. Palieraki. 2016. "In-plane and out-of-plane response of a masonry infill divided into smaller wallettes." In *Proc., 16th Int. Brick and Block Masonry Conf.*, 1367–1373. Leiden, The Netherlands: Taylor & Francis Group.

Vintzileou, E., and V. Palieraki. 2007. "Perimeter infill walls: The use of bed joint reinforcement or RC tie-beams." *Masonry Int.* 20 (3): 117–128.

Zarnic, R., and M. Tomazevic. 1988. "An experimentally obtained method for evaluation of the behavior of masonry infilled RC frames." In *Proc., 9th World Conf. on Earthquake Engineering*, 163–168. Tokyo: Japan Association for Earthquake Disaster Prevention.